Doctor Thesis

ES1 is a mitochondrial enlarging factor contributing to form mega-mitochondria in zebrafish cones

(ES1 はゼブラフィッシュ錐体のミトコンドリアの拡大を促進し、
メガミトコンドリアの形成に寄与する)

Sensory Transduction Group (Prof. Kawamura)
Nanobiology Laboratories
Graduate School of Frontier Biosciences
Osaka University

Takamasa Masuda
March 2016

論文内容の要旨

ES1 is a mitochondrial enlarging factor contributing to form mega-mitochondria in zebrafish cones.
(ES1 はゼブラフィッシュ錐体のミトコンドリアの拡大を促進し、メガミトコンドリアの形成に寄与する)

脊椎動物の網膜には、桿体と錐体の二種類の視細胞が存在する。視細胞はエネルギー消費が多く、外節近傍のエリプソイドにミトコンドリアのクラスターを形成してエネルギーを賄っている。明所視を担う錐体は、暗所視を担う桿体に比べてより多くのエネルギーを消費すると考えられており、その高いエネルギー需要と符合するように、一般に錐体エリプソイドには桿体よりも大きなミトコンドリアクラスターが形成されている。ゼブラフィッシュを含む一部の動物種の錐体には、直径が 2 μm を超える巨大なミトコンドリア (メガミトコンドリア) が存在する。メガミトコンドリアは、その高いエネルギー需要を補っていると考えられているが、その形成メカニズムは未だ不明である。

当研究室は、コイの精製錐体試料中に多量に含まれるタンパク質 ES1 に着目してきた。ES1 は、ゼブラフィッシュ網膜の主要なタンパク質として同定され、錐体内節に局在することが報告されている。その一次配列から、ES1 はミトコンドリアに局在することが予測されたものの、その生理的役割に関する知見はこれまで得られていない。

今回の研究で私は、ES1 が錐体メガミトコンドリアの形成に関わる因子の候補であると考えて、ES1 の機能解析を行った。まず、ES1 に対する抗体や RNA プローブを用いた局在解析から、ES1 はゼブラフィッシュの錐体に特異的に発現し、ミトコンドリアの局在することを示した。次にモルフォリノを用いた ES1 の発現阻害実験を行った結果、4 日齢稚魚において錐体ミトコンドリアの縮小が観察された。続いて、*Tol*2 transposon system を用いて、ES1 を桿体で異所的に発現するトランスジェニック系統を作製し、桿体ミトコンドリアの表現型解析を行った。その結果、個々のミトコンドリアの拡大が観察され、中には直径が 2 μm を超えるミトコンドリアも見られた。これらの結果から、ES1 はミトコンドリアの拡大に寄与し、錐体メガミトコンドリアの形成に寄与することが示唆された。さらに、ES1 発現桿体に対して次世代シーケンサーを用いた網羅的遺伝子発現解析を行った。その結果、ES1 発現桿体では ES1 を発現してない陰性対照の桿体に比べて、ミトコンドリア関連遺伝子の発現が上昇していた。そのことから、ES1 の導入によりミトコンドリア局在タンパク質の発現が増加し、その結果、ミトコンドリア新生が亢進したことが示唆された。さらに AMPK のリン酸化量および細胞内 ATP 量を測定した結果、ES1 発現桿体内の ATP 含有量は野生型桿体に比べて多いことが示された。これらのことから、ES1 はミトコンドリアの拡大を通して錐体のエネルギー産生に寄与することが示唆された。

Contents

Abstract

Mitochondrial mass and morphology differ in diverse cell types. High energy-demanding cells such as skeletal muscle cells, cardiac myocytes, and neuronal cells including photoreceptors, have high mitochondrial content. Cones, one of the photoreceptors in vertebrates mediating daylight vision, also require high energy to generate continuous light response, and so are endowed with numerous mitochondria. Besides, huge mitochondria named mega-mitochondria are observed in cones of certain mammals and fish; however, molecular mechanisms by which such curious mitochondria were formed in cones are not understood. Here I provide several lines of evidence showing that ES1 is a novel mitochondria-enlarging factor contributing to form cone mega-mitochondria in zebrafish (*Danio rerio*) retina. *In situ* hybridization, immunohistochemistry and immunoelectron microscopy showed that ES1 was specifically expressed in cones and localized to mitochondria including mega-mitochondria. Knockdown of ES1 using antisense morpholinos (MOs) markedly reduced the mitochondrial size in cone of 4dpf (days post fertilization) larvae. In contrast, significant increases in rod mitochondrial size and total mitochondria mass were observed in transgenic (TG) zebrafish ectopically expressing ES1 in rods. These results from loss-of- and gain-of-function experiments revealed that ES1 is a necessary and sufficient factor for the mitochondrial enlargement and formation of mega-mitochondria. Additionally, lower phosphorylation levels of AMP-activated protein kinase α (AMPKα) and higher cellular ATP levels were observed in the ES1-expressing rods, indicating that the enlarged mitochondria by ES1 were capable of high energy production. Furthermore, transcriptome analysis revealed that expression of mitochondria-related genes was up-regulated in the ES1-expressing rods, indicating that ES1 facilitates mitochondrial biogenesis via induction of mitochondrial proteins expression. Consequently, I propose that ES1 is a novel mitochondrial protein contributing to mitochondrial enlargement and mitochondrial biogenesis.

Introduction

The first step of vision is that photoreceptors in retina receive light from outside. Signal of the received light is converted into membrane potential change in the photoreceptors and sequentially transferred to subsequent neurons toward visual cortex in brain, where visual sensation is generated. For vision under wide range of light intensity, vertebrates use two types of photoreceptor, rods and cones. Rods are highly light-sensitive photoreceptors expressing rod visual pigment, rhodopsin, a light-receiving protein of rod-type, and are used for night vision. Cones are less light-sensitive photoreceptors expressing cone visual pigment, and used for daylight vision. Cones show much briefer light responses than rods, providing higher time resolution in daylight vision. In the cone-mediated vision, many vertebrates including us can distinguish colours. This is because, in our retina, there are several types

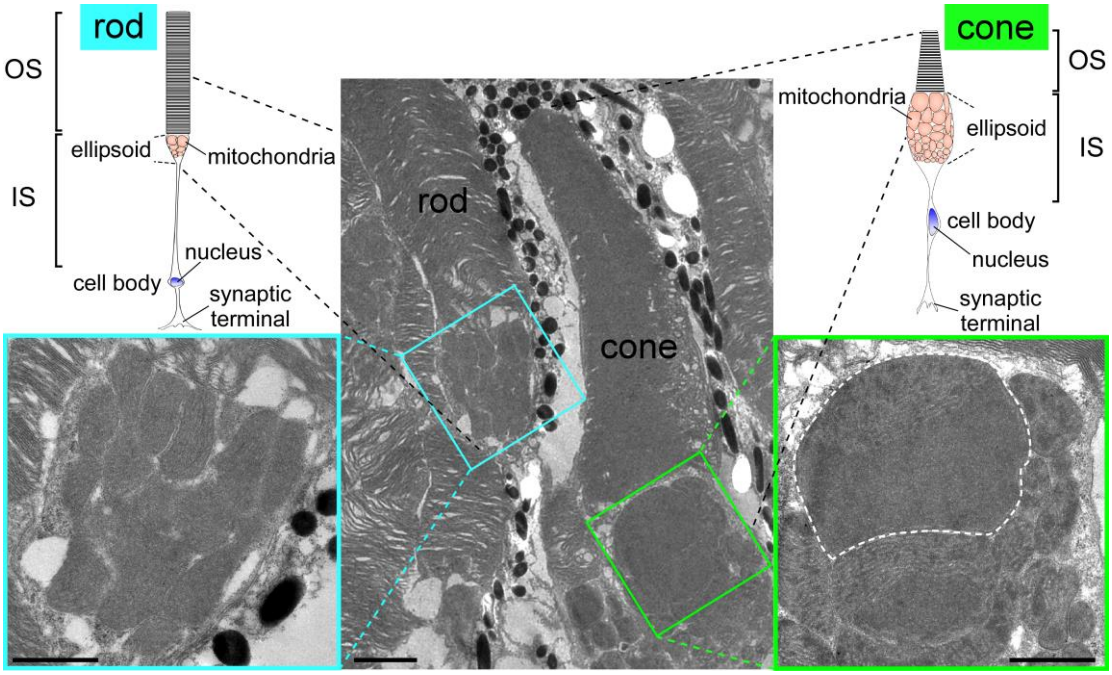

Figure 1 Mitochondria in photoreceptors.

The morphologies of rod (left) and cone (right) are described as illustrations. Mitochondria are packed within ellipsoid in inner segment. Electron microscopic images represent mitochondria in rod ellipsoid (left) and cone ellipsoid (right) of adult zebrafish. In cones, a mega-mitochondrion (over 2 μm in diameter, white dashed line) is observed in the distal portion of ellipsoid. Scale bars, 1μm.

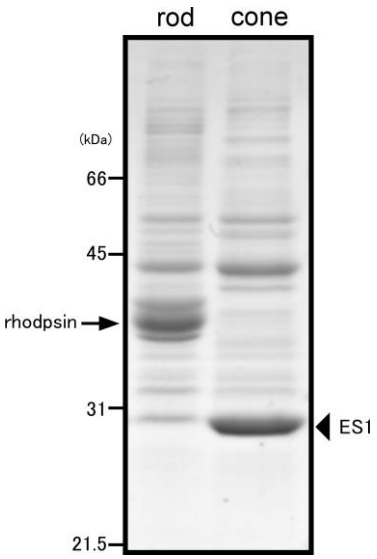

Figure 2 ES1 is the major component in cones.
Comparative analysis for protein components in carp rods and cones was performed by SDS-PAGE. In contrast to rods which possess rhodopsin as the dominant component, ES1 composes a large part of proteins expressed in cones. This figure was modified from Figure 3 in Komatsu Y, 2006.

of cones exressing different cone visual pigments with distinct absorption maxima, contrasting to night vision mediated by only single type of rods. Human has three types of cone expressing red-, green- and blue-light-receiving cone pigments, and fish including zebrafish has UV-sensitive cones in addition to the three types.

Both rods and cones are high energy-consuming cells (Alm A, 1992; Schmidt M *et al*., 2003; Linton JD *et al*., 2010). The major demand of ATP in photoreceptors is considered to maintain resting membrane potential by pumping out cations which enter through ion channels in dark (Okawa H *et al*., 2008). To generate briefer light responses, light-stimulated cones quickly restart cation influx by opening of the ion channels closed, and accordingly, cones must continuously pump them out in daylight vision where rods are saturated. Thus, cones require more energy than rods (Okawa H *et al*., 2008). Accommodating with their respective properties in both light response and energy demand, rods and cones are also endowed with distinctive morphological features. Rods represent long and thin shape with long outer segment containing a lot of rhodopsin (Fig. 1). Cones, on the other hand, represent short and thick shape with short outer segment and expanded ellipsoid, an apical region of inner segment. Ellipsoids are filled with mitochondria forming mitochondrial cluster. Cones possess higher total mass of mitochondria than rods as shown in many vertebrate species (Fig.

1, Kageyama GH & Wong-Riley M, 1984; Hoang QV *et al*., 2002; Perkins GA *et al*., 2003). These mitochondria are supposed to meet the higher energy demand in cones as described above. In addition, extremely large mitochondria, mega-mitochondria exceeding 2 μm in diameter, are observed in cones of certain species such as shrew and zebrafish (Fig. 1, Nag TC & Bhattacharjee J, 1995; Lluch S *et al*., 2002; Kim J *et al*., 2005; Knabe W & Kuhn HJ, 1996). Although they are supposed to contribute to high energy production, molecular mechanisms by which such huge mitochondria are formed in cones are not understood.

Since retinas generally contain cones less in number than rods, purification of cones has been difficult in terms of quantity necessary for studies at the molecular level. Using carp retinas, a method to purify cones has been first established in our laboratory by a Percoll density-gradient method (Tachibanaki S *et al*, 2001). The method has revealed that a 28k Da protein is dominantly expressed in carp cones, in contrast to rods expressing rhodopsin dominantly (Fig. 2). Komatsu Y, in our laboratory, has identified the protein as ES1 by N-terminal amino acid sequence analysis (Komatsu Y, 2006). ES1 has been found abundantly in the zebrafish retina and specifically in cone ellipsoids (Chang H & Gilbert W, 1997). ES1 accounts for approximately 45% of all proteins in purified cones (Komatsu Y, 2006), implying that ES1 can play important physiological roles in cones. Besides, orthologues of ES1 are conserved across species from *E. coli* (σ cross-reacting protein 27A, SCRP27A) to human, with strong similarities ranging from 77% to 81%, implying their significant roles conserved among prokaryote and eukaryotic mitochondria (Scott HS *et al*., 1997). However, any functional analyses of ES1 or its orthologues have not been executed so far. These facts led me to investigate the physiological role of ES1 in cones.

In the present study, using zebrafish, I showed that ES1 localization is restricted in cone mitochondria. Furthermore, loss-of and gain-of function analyses clearly demonstrated that ES1 is a mitochondria-enlarging factor and contributes to

form mega-mitochondria in cones. Transcriptome analysis for ES1-expressing rods strongly suggested that ES1 facilitates mitochondrial biogenesis via up-regulation of ERRα, which induces mitochondrial protein expression. Additionally, cellular energy level was elevated in ES1 expressing rods, indicating ES1 contribution to high energy production.

Results

ES1 is localized in cone mitochondria.

Aiming to elucidate physiological roles of ES1, I firstly investigated ES1 localization in zebrafish. Both RT-PCR and immunoblot analyses demonstrated that expression of ES1 was restricted to eyes (Fig. 3a and b, respectively). Subsequently, *in situ* hybridization analysis revealed that ES1 mRNA was expressed only in cones in retina (Fig. 3c).

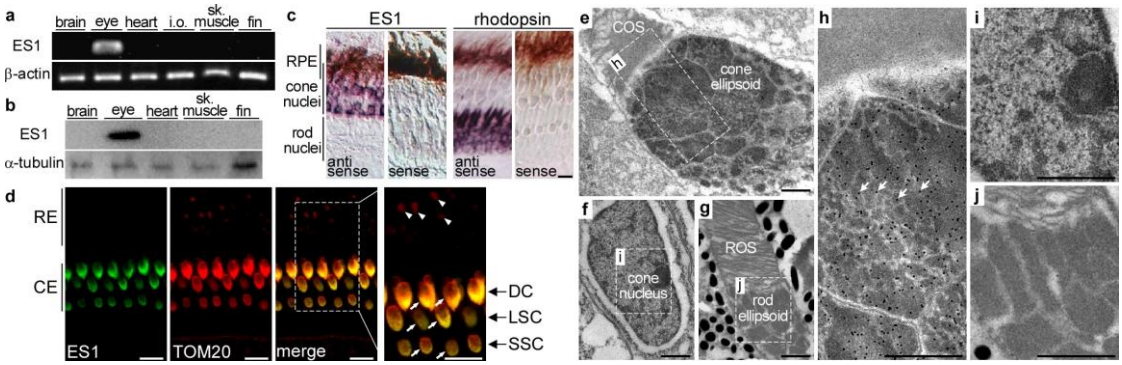

Figure 3 ES1 is specifically expressed in cones and localized to mitochondria.

(a) RT-PCR assay for ES1 gene expression in zebrafish tissues. Beta-actin was used as an internal control for a constant amount of RNA templates. i.o.: internal organs, sk. muscle: skeletal muscle. (b) Immunoblot assay with ES1 antibody in zebrafish tissues. Alpha-tubulin antibody was used as a loading control. sk. muscle: skeletal muscle. (c) *In situ* hybridization on adult zebrafish retina. ES1 mRNA was only detected around cone nuclei (purple staining, left panels). Rhodopsin probe was used as a rod maker (right panels). Dark-brown staining in RPE (retinal pigment epithelium) layer is due to endogenous melanin pigment. Scale bars, 10 μm. (d) Immunohistochemistry on adult zebrafish retina with ES1 (green) and TOM20 (mitochondrial marker, red) antibodies. ES1-immunoreactivity was detected in ellipsoids in all types of cones (i.e., double, long-single and short-single cones, arrows) but not in rod ellipsoids (arrow heads). Scale bars, 10 μm. RE: rod ellipsoid, CE: cone ellipsoid, DC: double cone, LSC: long-single cone, SSC: short-single cone. (e-j) Immuno-gold electron microscopy with ES1 antibody on adult zebrafish retina. Each panel shows a cone ellipsoid with an outer segment (in e), a cone nucleus (in f) or a rod ellipsoid with an outer segment (in g). Panel h, i and j are magnified views of the areas surrounded by dashed lines in e, f and g, respectively. A mega-mitochondrion was observed in the apical region of the cone ellipsoid (in e and h, adjacent to the outer segment). Arrows indicate gold particles in h. Scale bars, 1 μm in e-j. COS: cone outer segment, ROS: rod outer segment.

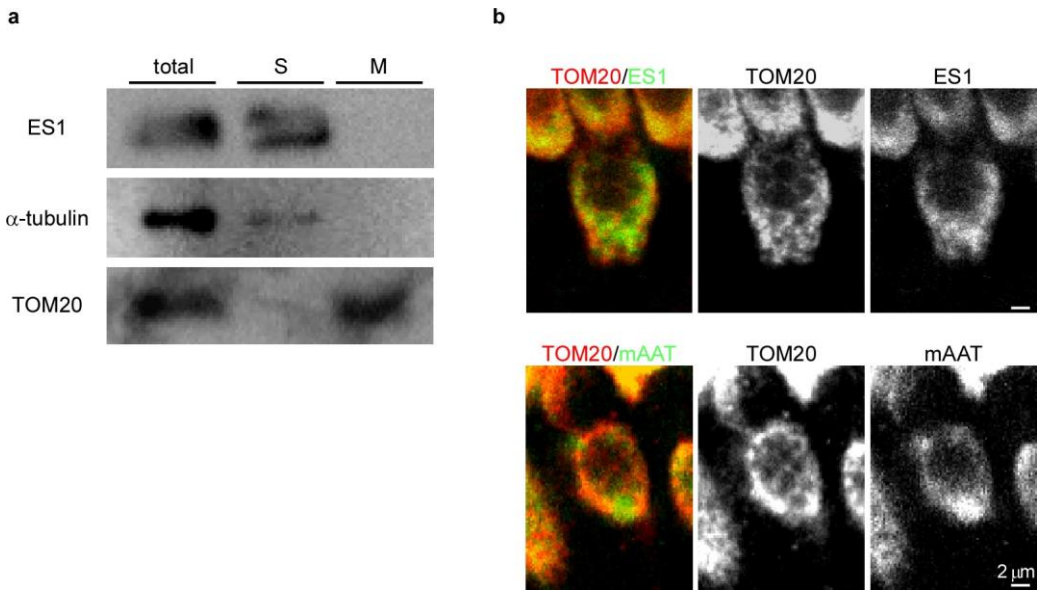

Figure 4 Subcellular localization of ES1 in zebrafish cones.

(a) Subcellular fractionation analysis for ES1. Immunoblotting analysis with anti-ES1 antibodies was performed using fractionated cells from retinas. Anti-alpha-tubulin and TOM20 antibodies were used as a marker for soluble fraction and membrane fraction, respectively. S: soluble fraction, M: membrane fraction. (b) Apparent heterogeneity of immunoreactivities in cone ellipsoid. High magnification views of double immunostainings of cone ellipsoids with TOM20/ES1 antibodies (upper panels) and TOM20/mAAT antibodies (lower panels). TOM20 antibody was used as a mitochondrial outer membrane marker to detect the outline of individual mitochondria. Both ES1- and mAAT-immunopositive signals were weaker at apical (upward direction) and central regions of the cone ellipsoids (right panels). In the same regions, TOM20 antibody depicted clear round patches >2 μm in diameter (middle panels), indicating the presence of mega-mitochondria. Scale bars, 2 μm.

Immunohistochemical analysis for zebrafish retina showed that ES1 is localized in cone ellipsoids but not rod ellipsoids (Fig. 3d). In a previous report, ES1 has been predicted to be localized to mitochondria because of a putative mitochondrial localization signal (MLS) present at the N-terminus (Shin JH *et al.*, 2004).Consistently, immunoreactivities of translocase of outer mitochondrial membrane 20 (TOM20) were also detected in cone ellipsoids, indicating localization of ES1 to mitochondria (Fig. 3d). Immunoelectron microscopy also demonstrated mitochondria-specific

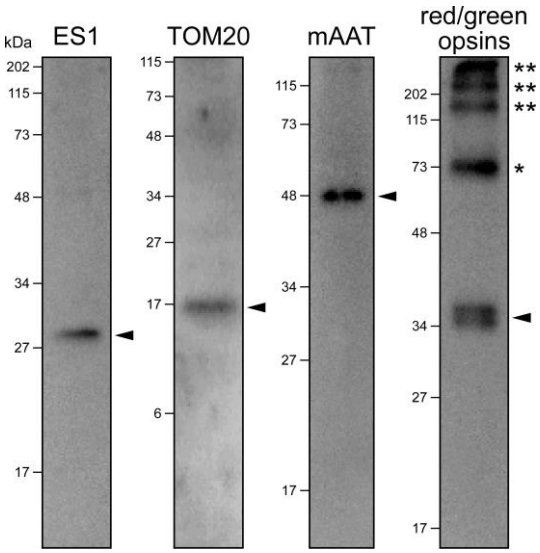

Figure 5 Immuno-specificities of antibodies used for immunohistochemical analyses. Immunoblottings were performed with anti-ES1, TOM20, mAAT and red/green opsins antibodies on lysate from the zebrafish eyes. Anti-ES1, TOM20 and mAAT antibodies showed only single bands (arrowheads), which correspond to the calculated molecular masses of each protein. Anti-red/green opsins antibody showed multiple bands which correspond to monomers (arrowhead), dimers (single asterisk) or multimers (double asterisks) of red/green opsins as previously reported (Ma J *et al.*, 2001).

localization of ES1 (Fig. 3e-j). ES1-immunopositive signals were uniformly distributed throughout all mitochondria in cone ellipsoids including mega-mitochondria (Fig. 3e, h). By immunoblot analysis after cell fractionation, ES1-immunoreactivity was detected in a soluble fraction but not a membrane fraction, suggesting that ES1 is present in mitochondrial matrix and/or intermembrane space (Fig. 4a). In contrast to the uniform distribution of ES1 in mitochondria observed in electron microscopy, at higher magnification under the light microscope, ES1-immunopositive signals were weaker at apical (adjacent to outer segment) and central regions of the cone ellipsoids where mega-mitochondria are located (Fig. 4b). This is probably due to low antibody permeability to access inside of mega-mitochondria because similar immunostaining patterns were observed with antibody against mitochondrial aspartate aminotransferase (mAAT), a mitochondrial matrix-marker protein (Fig. 4b). Immuno-specificities of antibodies used for immunohistochemical analyses were confirmed by immunoblot analyses (Fig. 5).

ES1 paralogues in zebrafish.

In silico screening using BLAST (http://blast.ncbi.nlm.nih.gov/Blast.cgi) revealed that zebrafish express three paralogues of ES1 (Gene ID: NM_001017662, XM_688586, XM_693418). According to EST profile of Unigene (www.ncbi.nlm.nih.gov/UniGene), these orthologues were expressed in various

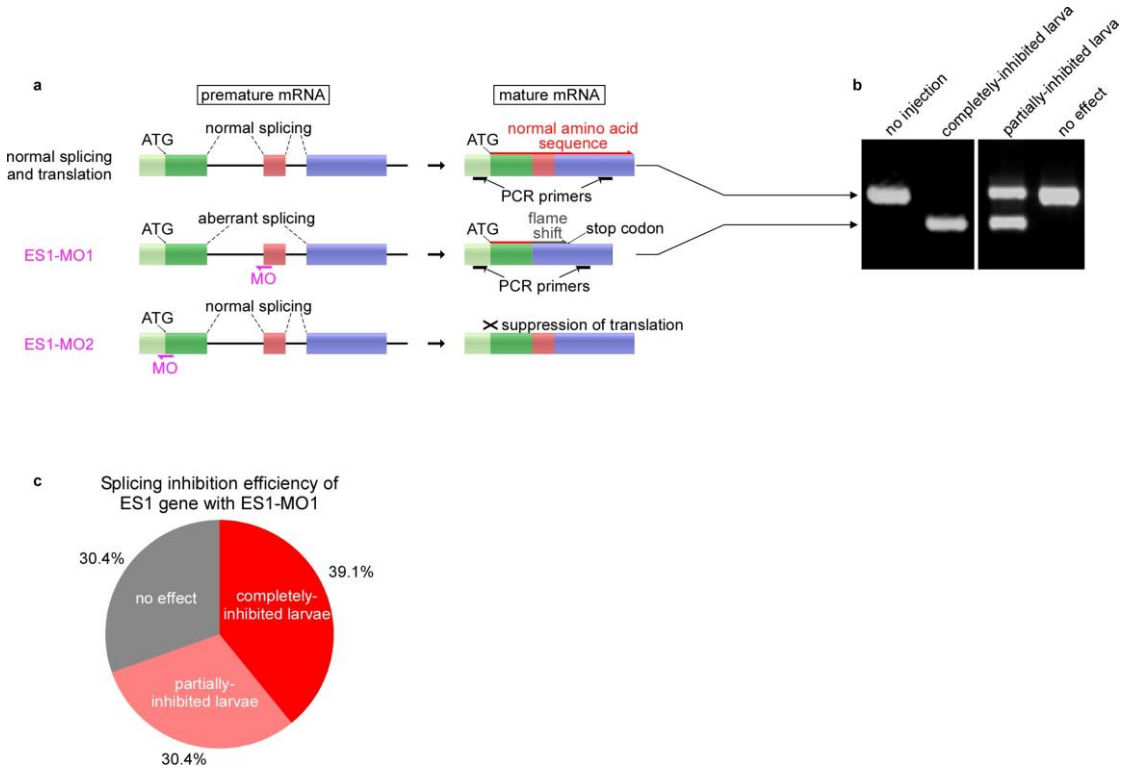

Figure 6 Two knocking-down strategies for ES1 by using MOs.

(a) Schematic drawings of the exon-intron structure of the ES1 gene and expected effects of two MOs. Thick coloured bars and thin lines indicate exons and introns, respectively. ES1-MO1 was designed to hybridize to an intron-exon boundary, leading to an exon-skipping to form a frame-shifted mRNA coding only a short aberrant sequence (24 amino acids) following N-terminal mitochondrial localization signal (23 amino acids). ES1-MO2 was designed to hybridize in close proximity to the translation initiation site of ES1 mRNA and to suppress the translation. (b) Representative results of RT-PCR assay evaluating the effect of ES1-MO1. Template RNAs were extracted from larvae at 4 dpf stage. The upper band was derived from the normally-spliced mRNA and the lower band was derived from aberrantly-spliced mRNA. (c) Splicing inhibition efficiency of ES1 transcript with ES1-MO1. Splicing was completely inhibited (red) in 39%, partially inhibited (pink) in 30% and not inhibited (gray) in 30% of ES1-MO1-injected larvae. n=23. Dead or malformed larvae were eliminated from the calculation.

tissues including eyes. By using bioinformatic software MITOPRED (Guda C *et al*., 2004 a; Guda C *et al*., 2004 b), the paralogue exhibiting the highest homology with ES1 (NM_001017662, 51.9 % identity of amino acid sequence) is predicted to be localized in mitochondria but the other paralogues are not, implying that this paralogue can be substituted for ES1 in diverse tissues.

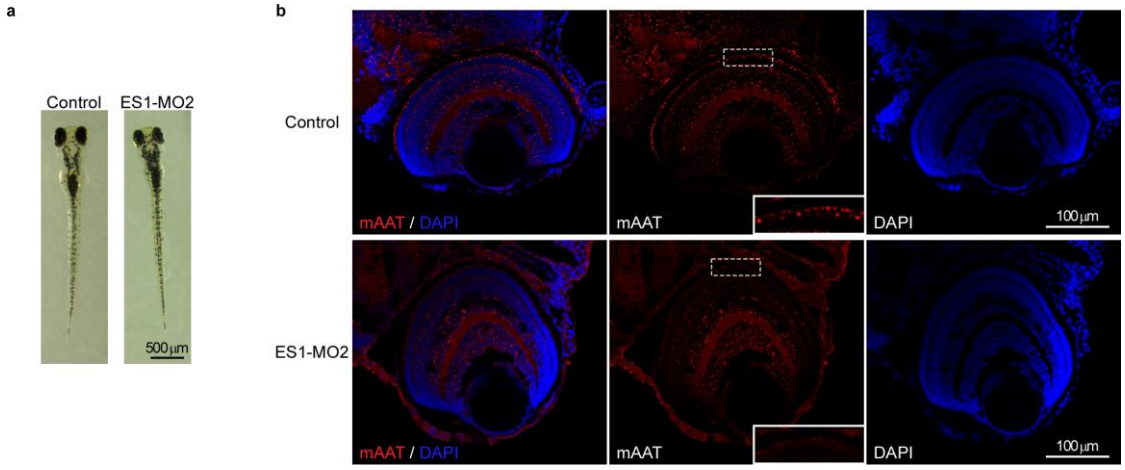

Figure 7 Morphology of MO-injected larvae.
(a) Whole body images of control MO- and ES1-MO2-injected 4 dpf larvae. (b) Immunohistochemistry of whole eye sections of control MO- and ES1-MO2-injected 4dpf larvae with mAAT antibody (red). Nuclei were stained with DAPI (blue). Immunopositive signals for mAAT were reduced only in cone ellipsoid layer (see dashed boxes and their magnified views shown in insets) of ES1-MO2-injected larvae compared to the control larvae.

ES1 knockdown reduced mitochondrial size in cones.

To elucidate physiological roles of ES1, knockdown approach was performed with MOs. The inhibiting effect of MOs injected into fertilized eggs is maintained until 4-5 dpf. At the time point, expression of all ES1 paralogues were detected by RT-PCR (data not shown). To avoid the side effect for them, MOs against ES1 transcript were designed without using sequences highly conserved in ES1 and the ES1 paralogues. For the knockdown analysis, I used two types of MOs against ES1, namely ES1-MO1 and ES1-MO2. ES1-MO1 was designed to generate a frame-shifted

mRNA by inhibiting a normal splicing and used to estimate the inhibition efficiency, and ES1-MO2 was designed to suppress translation (Fig. 6a). The ES1-MO1-mediated splicing inhibition was confirmed by RT-PCR in larvae at 4 dpf stage (Fig. 6b, c). Eye size of ES1-MOs-injected larvae was slightly decreased compared with that of

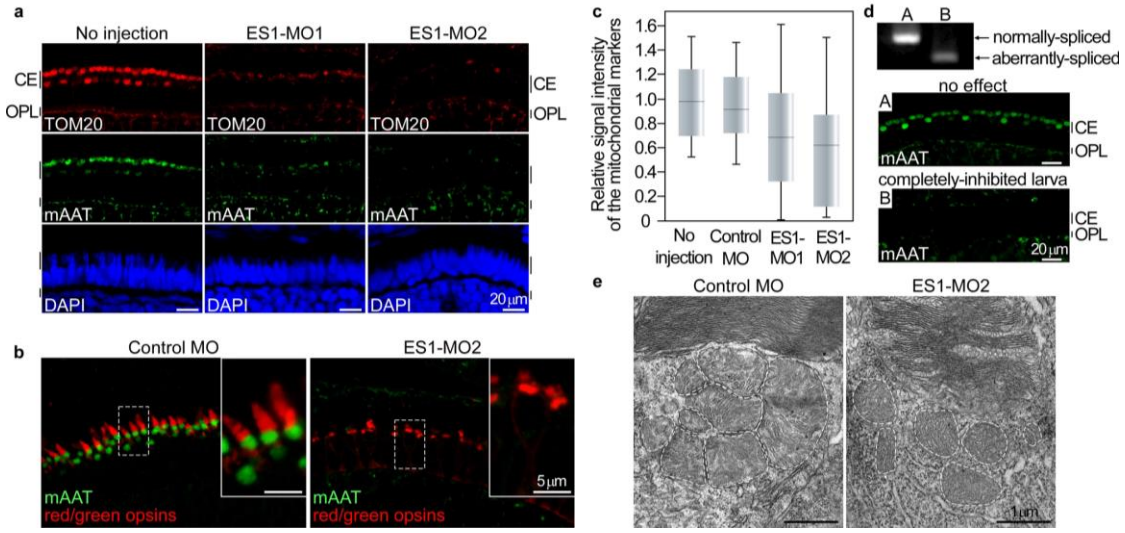

Figure 8 Knocking-down of ES1 resulted in formation of smaller mitochondria in cones. (a) Immunohistochemistry of retinal sections from ES1-MOs-injected or non-injected larvae at 4 dpf stage with both TOM20 (red) and mAAT (green) antibodies. Nuclei are stained with DAPI (blue). CE: cone ellipsoid, OPL: outer plexiform layer. (b) Immunohistochemistry with red/green opsins (cone outer segment marker, red) and mAAT (green) antibodies. The inset in each panel is a magnified view of the area surrounded by the dashed line. (c) Quantification of relative signal intensities of the mitochondrial markers from the cone ellipsoid layer of each MO-injected class; no injection (n=28), control MO (n=23), ES1-MO1 (n=37) and ES1-MO2 (n=23). Data are presented as box-whisker plots showing the median, quartiles and range. Mean value of no injection class was set to 1.0. (d) A paired RT-PCR (top) and immunohistochemical analysis (middle and bottom) in a single larva using a single eye for each analysis without (A) or with (B) the knock down effect of ES1-MO1. A completely-inhibited larva showed the relative immunopositive signal intensity of 0.20 (B), whereas a larva representing no inhibition showed 0.77 (A). (e) Representatives of electron microscopic images of cone mitochondria of control MO-injected (left panel) or ES1-MO2-injected (right panel) larvae at 4 dpf. Dashed lines outline each mitochondrion. The images without the outlines are shown in Fig. 9.

control-MO-injected larvae, suggesting that ES1 depletion affected eye growth in early stages (Fig. 7). Any other obvious differences were not observed in whole body shape or retinal structure between the ES1-MOs and control-MO-injected larvae (Fig. 7). In some population of larvae injected with either of the two ES1-MOs but not a control MO, immunoreactivities for two mitochondrial marker proteins, i.e., TOM20 and mAAT, were significantly reduced in the cone ellipsoid layer (Fig. 8a). To determine whether this phenotype is due to loss of the ability to differentiate into cones, red/green-sensitive opsins antibody was used as a cone differentiation maker. Cells representing reduced mitochondrial marker signals were immunopositive to the antibody in retinas of ES1-MO injected zebrafish, confirming the differentiation into cones (Fig. 8b). Quantification of immunoreactivities to the mitochondrial markers demonstrated that average of signal intensity was reduced in the ES1-MOs-injected group (Fig. 8c). Values of the signal intensities were scattered in a wide range covering the range of control MO-injected group, and that of the population of the larvae showing weaker signals than the control group was 35% in the ES1-MO1-injected group. This proportion well agreed with the portion of the larvae whose normal splicing of ES1 transcript was completely suppressed (39%, Fig. 6c). To evaluate more directly such an effect of ES1-MO1 on cone mitochondria, a paired RT-PCR and immunohistochemical analysis in a single larva using a single eye for each measurement was performed. As a result, a completely knocked-down larva (larva B in Fig. 8d) showed only weak immunoreactivities to the mitochondria markers in the cone ellipsoid layer (the relative signal intensity was 0.2), indicating strongly that inhibition of ES1 expression causes the loss of mitochondrial signals. ES1-MO2 induced the same phenotype more effectively (Fig. 8a, c), excluding the possibility of off-target effects. Subsequently, I observed the size of individual mitochondria in cone ellipsoids of the ES1-MOs-injected larvae by electron microscopy. Compared with the control MO-injected larvae, smaller mitochondria were observed in the cone ellipsoid both of ES1-MO1- and -MO2-injected larvae (Fig. 8e and Fig. 9). These results revealed that ES1 is necessary to form large mitochondria in cones.

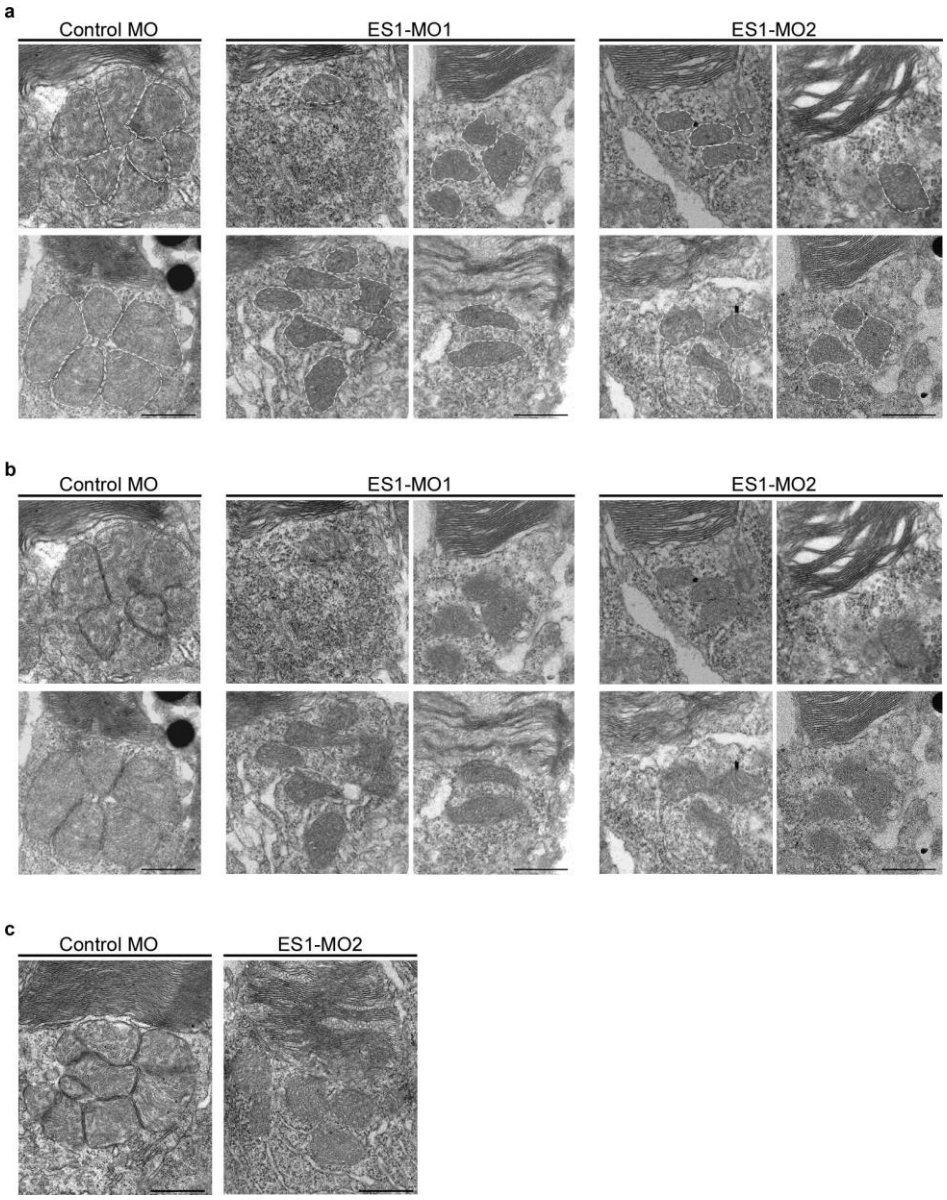

Figure 9 Morphology of cone mitochondria of MO-injected larvae.

(a) Representative electron microscopic images of cone mitochondria of control MO-injected (left panels), ES1-MO1-injected (center panels) or ES1-MO2-injected (right panels) larvae at 4 dpf. Dashed lines outline each mitochondrion. (b) Images of a without dashed lines. (c) Images of Fig. 8e without dashed lines. Scale bars, 1 μm.

CRISPR/Cas9-madiate ES1 knockout (KO) induced cell death in larvae retina.

Although MO is an accepted alternative genomic lesions, there are reports showing that KO zebrafish of most genes did not display readily observed embryonic phenotype induced by MO (Varshney GK *et al.,* 2015 and Kok FO *et al*., 2014). The reports insist that MO-mediated phenotypes are the results of off-target inhibition. To investigate whether the phenotype of MO-mediated ES1 knockdown was a result of off-target inhibition or not, I tried to generate ES1 KO zebrafish using CRISPR/Cas9 system. I designed two sgRNAs targeting two different positions in the first exon of ES1 gene (Fig. 10a, sgRNA ES1-1 and -2). Either of these sgRNAs was co-injected with Cas9 mRNA into 1 cell-stage eggs. T7 Endonuclease I (T7E1) assay and heteroduplex mobility analysis (HMA) showed induction of mutations in ES1 gene by the injection (Fig. 10b, c). Sequencing analysis for a fish injected with sgRNA ES1-1 confirmed mutations at near the targeting sequence (Fig. 10d). In retinas of 4 dpf larvae injected with the sgRNAs (F_0, mosaic), immunoreactivities to the mitochondria marker were slightly but not significantly weak in cone ellipsoid layer and, similarly, immunoreactivities to cone marker were also slightly reduced (Fig. 10e). Contrary to the phenotype observed in MO-injected larvae retina, reduced mitochondrial marker signal in cones (Fig. 8b), cones displaying weak mitochondria marker signal were not observed in sgRNAs injected larvae retina. This result indicates that ES1 KO cones did not represent phenotype of reduction of mitochondrial size as observed in MO-injected larvae. On the other hand, TUNEL positive signals were significantly increased in sgRNAs injected larvae retina compared to control larvae (Fig. 10f, g). These results suggest that ES1 KO induced apoptotic cell death rather than mitochondrial size reduction.

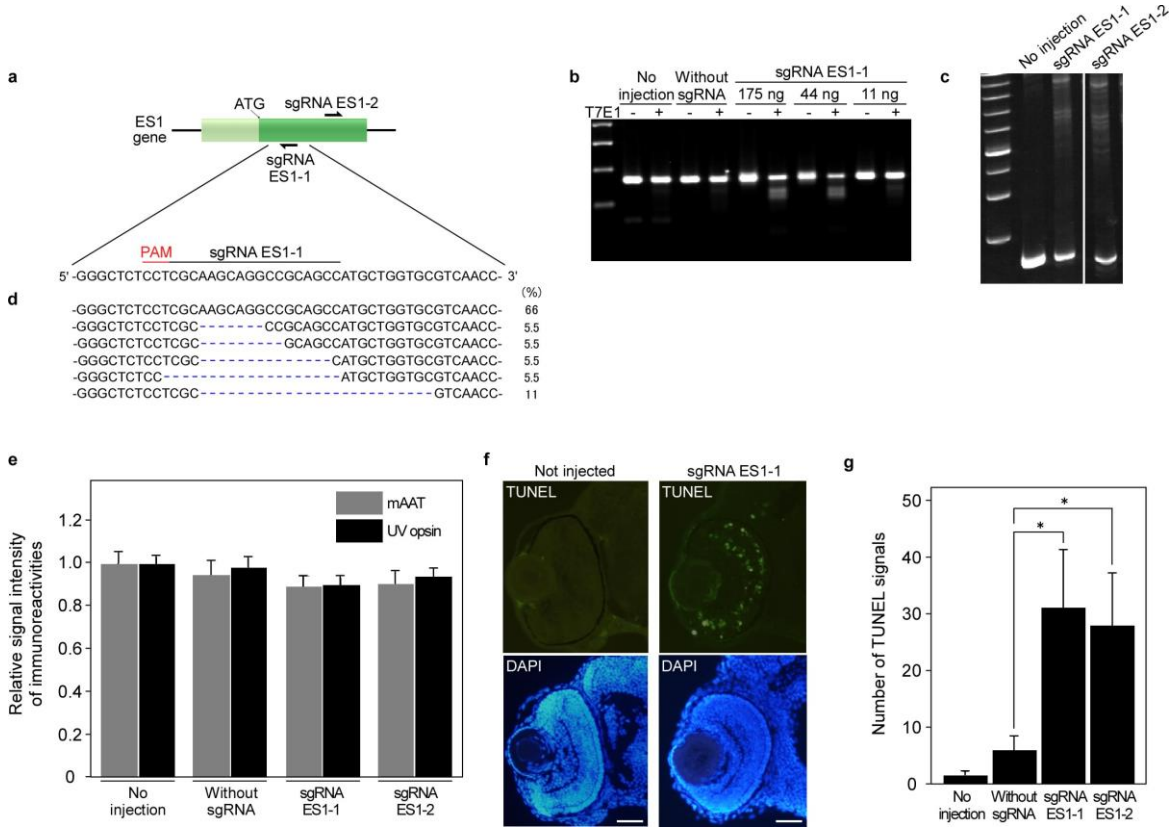

Figure 10 CRISPR/Cas9 system-mediated ES1 knockout.

(a) Schematic drawing of targeting region of sgRNAs against ES1 gene. Both sgRNA ES1-1 and -2 were designed to target sequences immediately downstream of initiation codon in the first exon. The targeted sequence of sgRNA ES1-1 and the protospacer adjacent motif (PAM) sequence are indicated by red and black line, respectively. (b) Detection of mutations in ES1 genes by T7E1 assay. Embryos injected only Cas9 mRNA were used as control (without sgRNA). Genomes exracted from 5 embryos at 24 hpf were subjected for the T7E1 assay. The amounts of the sgRNA used for the injection were indicated on the top of the image. (c) Detection of mutations in ES1 genes by HMA. Genomes extracted from an embryo at 24 hpf injected 44 ng of each sgRNAs were subjected for HMA. In lanes for sgRNAs injected larvae, bands of heteroduplex were up-shifted (d) Mutation frequency induced by sgRNA ES1-1. Sequences adjacent to sgRNA ES1-1 targeting region of a larvae injected with 44 ng sgRNA ES1-1 showed deletion mutations. (e) Relative signal intensity of immunoreactivities of mAAT and UV opsin antibodies. Signal intensity was measured around cone ellipsoid layer in 4 dpf larvae retina. Values are means ± S.E., n=5 for all groups. (f) Representative images of TUNEL assay for 3 dpf larvae retinal sections of 3 dpf larvae. Nuclei were stained with DAPI. Scale bar, 50μm. (g) The number of TUNEL positive signals in retinal sections. Values are means ± S.E., *P< 0.05 in Student's t-test. n=7 for no injection, n=6 for both without sgRNA and sgRNA ES1-1, and n=5 for sgRNA ES1-2.

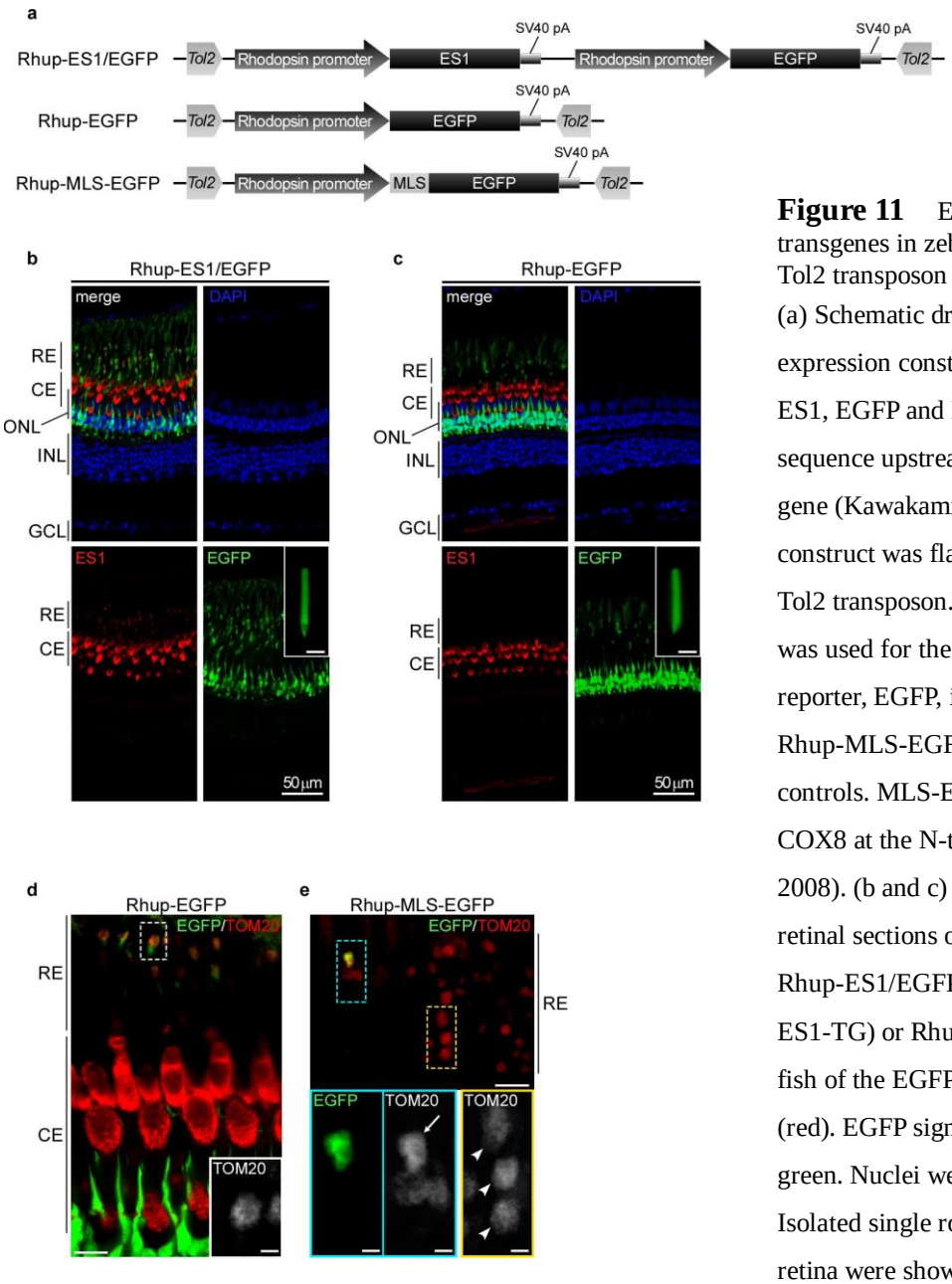

Figure 11 Ectopic expression of transgenes in zebrafish rods with the aid of Tol2 transposon system.

(a) Schematic drawings of Tol2-based expression constructs. Coding sequences of ES1, EGFP and MLS-EGFP were driven by a sequence upstream 1,084 bp of rhodopsin gene (Kawakami K *et al.*, 2004) Each construct was flanked by inverted repeats of Tol2 transposon. Rhup-ES1/EGFP construct was used for the expression of ES1 and a reporter, EGFP, in rods. Rhup-EGFP and Rhup-MLS-EGFP constructs were used as controls. MLS-EGFP contains MLS of COX8 at the N-terminus (Kim MJ *et al.*, 2008). (b and c) Immunohistochemistries of retinal sections of TG zebrafish harboring Rhup-ES1/EGFP (b, F_0 mosaic fish of the ES1-TG) or Rhup-EGFP (c, F_1 non-mosaic fish of the EGFP-TG) with ES1 antibody (red). EGFP signals were represented in green. Nuclei were stained with DAPI (blue). Isolated single rod outersegments from each retina were shown in insets. Scale bars, 10 μm in the insets. (d and e) Immunohistochemistries of retinal sections of EGFP-TG (d) or TG harboring Rhup-MLS-EGFP (MLS-EGFP-TG; F0 generation; mosaic, e) with TOM20 antibody (red). The inset in d and the lower panels in e are magnified views of areas surrounded by dashed lines in d and in the top panel in e, respectively. In panel e, an ellipsoid of MLS-EGFP-TG rod and ellipsoids of wild-type rods are indicated by an arrow and arrow heads, respectively. Scale bars, 10 μm in the main panel of d and the upper panel of e, and 2 μm in the inset of d and the lower panels of e. RE: rod ellipsoid, CE: cone ellipsoid, ONL: outer nuclear layer, INL: inner nuclear layar, GCL: ganglion cell layer.

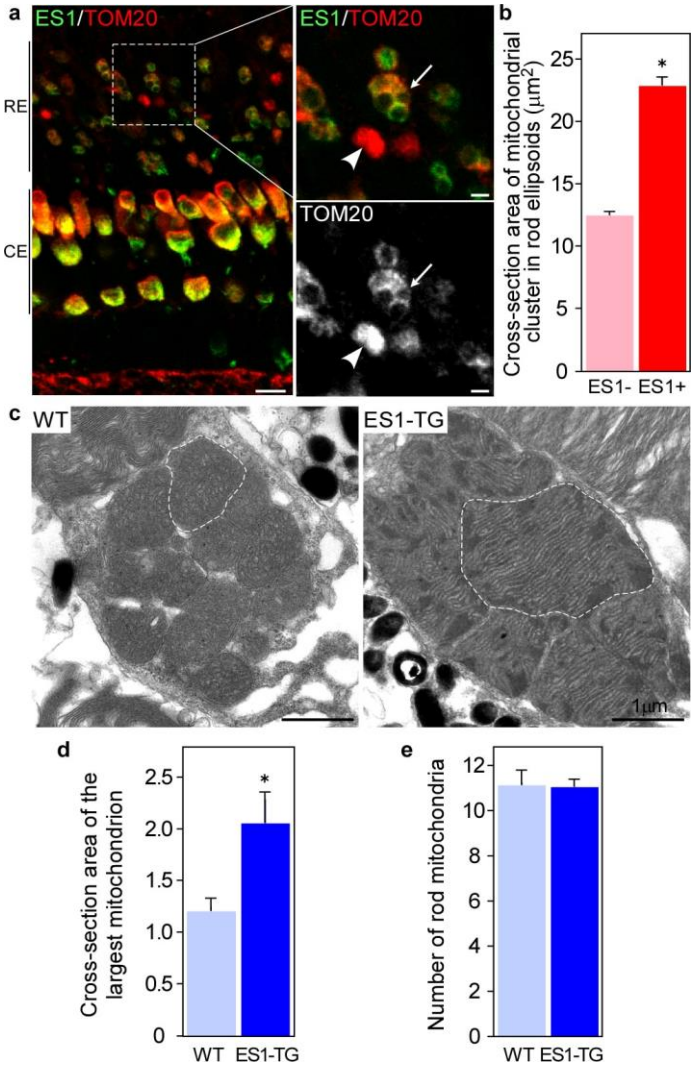

Figure 12 Ectopic expression of ES1 led mitochondrial enlargement in rods.
(a) Immunohistochemistry of retinal sections from adult ES1-TG zebrafish (F_0) with ES1 (green) and TOM20 (red) antibodies. Images are at a certain depth of confocal view. Right panels show a magnified view of merged image (upper) or TOM20 alone (lower). An arrow in each panel indicates a mitochondrial cluster in an ES1-expressing rod ellipsoid and an arrowhead indicates a mitochondrial cluster in a wild-type rod ellipsoid. As in the cone ellipsoids, immunopositive signals were weaker in the round patch in the ES1-expressing rods than the wild-type, presumably because of low antibody permeability of mega-mitochondria. Scale bars, 10 μm (left panel) and 2 μm (right panels). RE: rod ellipsoid, CE: cone ellipsoid. (b) Quantification of cross-section areas of mitochondrial clusters in rod ellipsoids. TOM20-immunopositive cross-section areas including immunonegative round areas were measured. Values are means ± S.E., *$P=2x10^{-31}$ in Student's t-test, n=120 for wild-type rods (ES1-) and n=142 for ES1-expressing rods (ES1+). (c) Representatives of electron microscopic images of mitochondria in wild-type (WT) rods (left panel) or ES1-TG rods (right panel). F_1 generation of ES1-TG zebrafish, in which all rods express ES1, was used. Dashed lines outline the largest mitochondrion in each view. (d) Size of mitochondria in ES1-TG and WT rods. Cross-section area of the largest mitochondrion in each rod ellipsoid was measured. Values are means ± S.E., *$P=2x10^{-4}$ in Student's t-test, n=9 for WT and n=25 for ES1-TG. (e) The number of mitochondria in each rod. Values are means ± S.E. n=23 for WT and n=38 for ES1-TG.

Ectopic expression of ES1 induced mitochondrial enlargement in rods.

From the results of the knockdown analysis above, I hypothesized that ES1 contributes to mitochondrial enlargement. To test this hypothesis, I next undertook a gain-of function analysis by generating TG zebrafish. Into fertilized eggs, I injected the DNA constructs designed to express ES1 ectopically in rods together with EGFP as a reporter (Fig. 11a). F_0 mosaic ES1-TG fish where ES1-immunoreactivities were detected in the ellipsoid of roughly a half of rods were successfully obtained (Fig. 12a left panel). Whole retinal structure was not changed in the ES1-TG fish and cell shape of the ES1-expressing rods was not changed except for the size of ellipsoids (Fig. 11b, c). Measurement of TOM20 immuno-positive area demonstrated that cross-section areas of mitochondrial clusters in ES1-positive rods were larger than those in wild-type rods (Fig. 12b). Such expansion of mitochondrial cluster was not observed in rods expressing EGFP alone or MLS-possessing EGFP (Fig. 11d, e). These results indicate that ectopic ES1 expression induced increase in total mitochondrial mass in rods. Besides, immunostaining for TOM20 showed distinctive appearance in the ES1-positive rod ellipsoids (layer RE): immunonegative round patches >2 μm in diameter were stacked like a bunch of raspberry (Fig. 12a, right panels), as seen in the apical and central regions of the cone ellipsoids (Fig. 4b). In contrast, no such immunonegative signals were observed in the wild-type rod ellipsoids (Fig. 12a). Since TOM20 is localized on the outer membrane of mitochondria (Ramage L *et al.*, 1993), its immunopositive signals are supposed to outline mitochondria. Therefore, such a difference in immunostaining pattern suggested enlargement of individual mitochondria in the ES1-positive rod ellipsoids. To elucidate the morphological changes of rod mitochondria in detail, electron microscopic observation was performed for ES1-TG retinas of F_1 generation, where all rods express ES1 ectopically. By electron microscopy, larger mitochondria were observed in ES1-TG rods compared to wild type rods (Fig. 12c, d). Additionally, mega-mitochondria, exceeding 2 μm in diameter, were observed in the ES1-TG rods, whereas no such huge mitochondria were observed in wild-type rods (Fig. 12c). Although the cristal membranes appears to be well aligned in the ES1-TG rod than the WT rod (Fig. 12c), significant difference

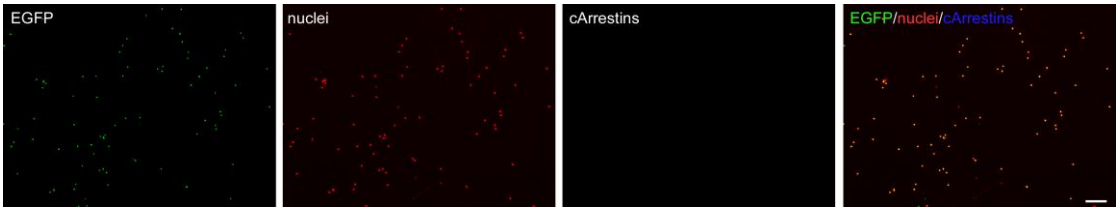

Figure 13 Purified rods by FACS.

Purified rods from ES1-TG or EGFP-TG retinas were subjected to immunocytochemistry with antibodies against cone-type Arrestin-1 and -2. Major part of EGFP-positive dots (green) contains nuclei (red, stained with DAPI). Antibodies against cone-type Arrestins, which are distributed entirely in cones were used as cone markers (blue). Ratio of cone contamination was a mere 0.28%. Scale bar, 100 μm.

was not observed in other images, suggesting that the structural variation is not related to the ES1 expression. In terms of the number of mitochondria, no significant difference was observed in each rod ellipsoid between the ES1-TG and the wild-type (Fig. 12e), indicating ES1-induced enlargement of individual mitochondria but not mitochondrial proliferation.

Expression of mitochondrial biogenesis-related transcription factors were up-regulated in the ES1-expressing rods.

To elucidate the molecular mechanisms by which the mitochondrial enlargement induced by ES1, I investigated gene expression changes in the ES1-expressing rods by transcriptome analysis. Rods were isolated from both ES1-TG and EGFP-TG (as the reference) retinas and subsequently purified by fluorescence-activated cell sorting (FACS). From the obtained rod fractions (>96% purity, Fig. 13), mRNA samples were extracted, and then subjected to high-throughput RNA sequencing (RNA-seq) using next generation sequencing (NGS) technology. To obtain data of gene expression levels and differentially expressed genes from the sequenced reads, computational analysis was performed using software such as Cufflinks and Cuffdiff (Trapnell C *et al.*, 2012). Scatter plot calculated from the RNA-seq data showed that the major portion of genes represents expression differences ranging from 0.5- to 2-fold in each condition (Fig. 14), indicating that

ectopic expression of ES1 did not induce a massive perturbation of gene expression in rods. Statistical analyses of the RNA-seq data revealed that 236 genes were significantly up-regulated (P <0.05) in the ES1-expressing rods (Table 1). Under more stringent criteria with Benjamini and Hochberg procedure (Q <0.05: Q represents adjusted P value for the multi testing), 42 genes were determined to be up-regulated (Table 1). On the other hand, both 229 genes (P <0.05) and 43 genes (Q <0.05) were determined to be down-regulated under each criterion (Table 1). Subsequently, Gene ontology (GO) and pathway enrichment analyses were performed to obtain the overview of attributes of the differentially expressed genes in the rods. These analyses demonstrated that genes classified into cytosolic ribosomal protein were mostly up-regulated, implying that ES1 facilitates protein synthesis activity in rods (Fig. 15a, Fig. 16a, and Table 2). Consistent with the mitochondrial enlargement electron transport chain and oxidative phosphorylation were also significantly up-regulated (Fig. 15a, Fig. 16a and Table 2).

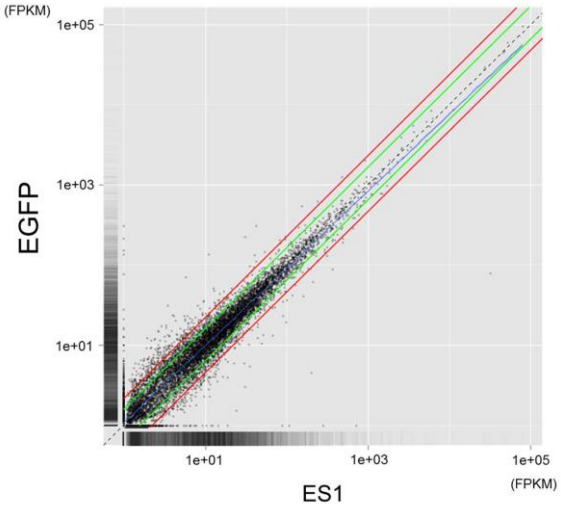

Figure 14 Variance of gene expression levels among ES1-TG and EGFP-TG samples.
Scatter plot where each dot represents expression level of a gene. The red and green lines indicate 2-fold and 1.5-fold expression difference between conditions, respectively. The blue line indicates the regression line. Data were calculated by CummeRbund according to FPKM values.

Table 1

Up-regulated genes in the ES1-expressing rods. Genes were sorted in descending order according to the value of fold change.

Genbank accession number	Gene symbol	Gene description	fold change	P value	Q value
NM_131039	es1	es1 protein	476.41	5.0E-5	0.005
NM_001006039	*samsn1b*	SAM domain, SH3 domain and nuclear localisation signals, 1b	49.90	5.0E-5	0.005
NM_131256	*nr6a1a*	nuclear receptor subfamily 6, group A, member 1a	8.60	5.0E-5	0.005
NM_001113659	zgc:198419	zgc:198419	6.80	0.002	0.084
NM_001085494	*hoxa13a*	homeo box A13a	5.19	5.0E-5	0.005
NM_131249	*evx1*	even-skipped homeobox 1	4.35	5.0E-5	0.005
NM_001244736	*cnbpa*	CCHC-type zinc finger, nucleic acid binding protein a	4.05	2.5E-4	0.017
NM_001109854	zgc:173594	zgc:173594	3.94	5.0E-5	0.005
NM_001077315	zgc:153911	zgc:153911	3.80	5.0E-5	0.005
NM_001002190	*rgcc*	regulator of cell cycle	3.80	5.0E-5	0.005
NR_036645	*rpph1*	ribonuclease P RNA component H1	3.77	0.010	0.206
NM_001037573	*actn2*	actinin, alpha 2	3.20	5.0E-5	0.005
NM_200303	zgc:56676	zgc:56676	3.16	0.031	0.332
NM_001020476	*dnmt3b*	DNA (cytosine-5-)-methyltransferase 3 beta	3.00	5.0E-5	0.005
NM_131295	*cpla2*	cytosolic phospholipase a2	2.90	5.0E-5	0.005
NM_001162502	*ncapd2*	non-SMC condensin I complex, subunit D2	2.90	5.0E-4	0.028
NM_001098760	*mul1b*	mitochondrial E3 ubiquitin ligase 1b	2.88	0.006	0.146
NM_001114720	*coq4*	coenzyme Q4 homolog (S. cerevisiae)	2.72	0.019	0.271
NM_213180	zgc:77112	zgc:77112	2.69	5.0E-5	0.005
NM_001126421	LOC565395	novel protein similar to DIRAS family, GTP-binding RAS-like 1 (diras1)	2.62	0.008	0.182
NM_131368	*smad5*	MAD homolog 5 (Drosophila)	2.60	5.0E-5	0.005

Genbank accession number	Gene symbol	Gene description	fold change	P value	Q value
NM_001003533	*bag3*	BCL2-associated athanogene 3	2.60	5.0E-5	0.005
NM_001076749	zgc:154164	zgc:154164	2.56	2.0E-4	0.015
NM_130936	*klfd*	Kruppel-like factor d	2.53	5.0E-5	0.005
NM_001128780	zgc:194423	zgc:194423	2.52	0.007	0.171
NM_200172	*mycb*	myelocytomatosis oncogene b	2.52	0.004	0.125
NM_001039144	*slc8a1b*	solute carrier family 8 (sodium/calcium exchanger), member 1b	2.42	5.0E-5	0.005
NM_199580	*hmmr*	hyaluronan mediated motility receptor	2.41	1.5E-4	0.012
NM_001002075	*ccne2*	cyclin E2	2.40	5.0E-5	0.005
NM_001045854	*pex11b*	peroxisomal biogenesis factor 11 beta	2.40	0.027	0.312
NM_001122611	*magi2*	membrane associated guanylate kinase, WW and PDZ domain containing 2	2.36	5.0E-5	0.005
NM_001077545	*gfm2*	G elongation factor, mitochondrial 2	2.33	7.5E-4	0.039
NM_001008644	*bmp2k*	BMP2 inducible kinase	2.31	5.0E-5	0.005
NM_199850	*c20orf24*	c20orf24 homolog (H. sapiens)	2.29	3.0E-4	0.019
NM_200167	*cpne3*	copine III	2.25	2.0E-4	0.015
NM_001014343	*sh2d5*	SH2 domain containing 5	2.17	0.002	0.067
NM_131237	*mxi1*	max interacting protein	2.16	5.0E-5	0.005
NM_200701	*wdr21*	WD repeat domain 21	2.13	0.032	0.336
NM_001110833	*ccdc94*	coiled-coil domain containing 94	2.12	0.018	0.267
NM_001201561	LOC555548	cardiac phospholamban-like	2.12	0.007	0.163
NM_199987	*jun*	jun proto-oncogene	2.10	5.0E-5	0.005
NM_200802	*clu*	clusterin	2.08	5.0E-5	0.005
NM_001020735	*pcyt1ab*	phosphate cytidylyltransferase 1, choline, alpha b	2.06	4.5E-4	0.026
NM_001007340	*ppm1db*	protein phosphatase 1D magnesium-dependent, delta isoform b	2.06	0.009	0.190

Genbank accession number	Gene symbol	Gene description	fold change	P value	Q value
NM_001014330	*mtmr1b*	myotubularin related protein 1b	2.05	7.5E-4	0.039
NM_001002743	*tk2*	thymidine kinase 2, mitochondrial	2.01	0.011	0.216
NM_001122705	*abl2*	v-abl Abelson murine leukemia viral oncogene homolog 2	2.01	0.010	0.208
NM_001001846	*pura*	purine-rich element binding protein A	2.00	0.003	0.104
NM_001077605	zgc:153381	zgc:153381	1.99	0.013	0.233
NM_001020551	*hmg20b*	high-mobility group 20B	1.99	0.020	0.278
NM_200117	*hist2h2l*	histone 2, H2, like	1.98	5.0E-5	0.005
NM_001102675	*pard6b*	par-6 partitioning defective 6 homolog beta (C. elegans)	1.98	0.048	0.385
NM_001017678	*ppie*	peptidylprolyl isomerase E (cyclophilin E)	1.97	0.014	0.244
NM_001113610	si:ch211-163l21.7	si:ch211-163l21.7	1.95	4.0E-4	0.024
NM_001005587	*crata*	carnitine O-acetyltransferase a	1.95	0.008	0.187
NM_001017840	*rasl11a*	RAS-like, family 11, member A	1.95	0.003	0.107
NM_001130625	zgc:194737	zgc:194737	1.95	0.005	0.131
NM_001077389	tfam	transcription factor A, mitochondrial	1.93	0.029	0.320
NM_212612	*ddx5*	DEAD (Asp-Glu-Ala-Asp) box polypeptide 5	1.91	5.0E-5	0.005
NM_200102	*pdcd8*	programmed cell death 8 (apoptosis-inducing factor)	1.91	1.5E-4	0.012
NM_212750	*junbb*	jun B proto-oncogene b	1.90	1.0E-4	0.008
NM_001109835	zgc:171937	zgc:171937	1.88	0.034	0.344
NM_199636	*rpl10a*	ribosomal protein L10a	1.87	2.5E-4	0.017
NM_200233	*hif1ab*	hypoxia-inducible factor 1, alpha subunit (basic helix-loop-helix transcription factor) b	1.86	5.0E-5	0.005
NM_001007765	*ndufs1*	NADH dehydrogenase (ubiquinone) Fe-S protein 1	1.86	2.0E-4	0.015
NM_199629	*nfkbiab*	nuclear factor of kappa light polypeptide gene enhancer in B-cells inhibitor, alpha b	1.84	1.0E-4	0.008
NM_001044985	si:dkey-72l14.3	si:dkey-72l14.3	1.84	0.002	0.065

Genbank accession number	Gene symbol	Gene description	fold change	P value	Q value
NM_213256	*ttyh2l*	tweety homolog 2, like	1.83	0.020	0.273
NM_200789	zgc:73324	zgc:73324	1.83	0.017	0.262
NM_001110286	*prkaa1*	protein kinase, AMP-activated, alpha 1 catalytic subunit	1.83	0.004	0.118
NM_001004542	zgc:91887	zgc:91887	1.82	0.008	0.187
NM_001098389	*hexim1*	hexamethylene bis-acetamide inducible 1	1.82	0.022	0.283
NM_200407	*ergic2*	ERGIC and golgi 2	1.82	0.044	0.379
NM_131073	*jak1*	Janus kinase 1	1.80	0.005	0.134
NM_199776	*ppp2r2d*	protein phosphatase 2, regulatory subunit B, delta isoform	1.80	0.005	0.137
NM_001002304	*twf1b*	twinfilin, actin-binding protein, homolog 1b	1.79	0.018	0.267
NM_001020543	zgc:109982	zgc:109982	1.79	0.011	0.210
NM_001083123	*ar*	androgen receptor	1.79	0.026	0.309
NM_200845	*rps17*	ribosomal protein S17	1.78	0.041	0.370
NM_213021	*glrx5*	glutaredoxin 5 homolog (S. cerevisiae)	1.78	0.035	0.349
NM_153662	*st8sia2*	ST8 alpha-N-acetyl-neuraminide alpha-2,8-sialyltransferase 2	1.78	7.5E-4	0.039
NM_213408	*slc25a22*	solute carrier family 25 (mitochondrial carrier: glutamate), member 22	1.78	0.023	0.293
NM_205553	zgc:55936	zgc:55936	1.78	0.023	0.292
NM_001017755	*ndufs3*	NADH dehydrogenase (ubiquinone) Fe-S protein 3, (NADH-coenzyme Q reductase)	1.76	0.009	0.191
NM_001045015	*ap3d1*	adaptor-related protein complex 3, delta 1 subunit	1.76	0.001	0.055
NM_201511	*cyp2p10*	cytochrome P450, family 2, subfamily P, polypeptide 10	1.75	0.047	0.384
NM_001045109	*furinb*	furin (paired basic amino acid cleaving enzyme) b	1.75	0.032	0.336
NM_199272	*esrp2*	epithelial splicing regulatory protein 2	1.75	2.0E-4	0.015
NM_001029956	*u2af2a*	U2 small nuclear RNA auxiliary factor 2a	1.74	0.005	0.145
NM_001089480	zgc:162310	zgc:162310	1.73	0.026	0.308

Genbank accession number	Gene symbol	Gene description	fold change	P value	Q value
NM_001077257	*foxo1a*	forkhead box O1 a	1.73	0.020	0.276
NM_001130603	*tmtc2*	transmembrane and tetratricopeptide repeat containing 2	1.73	0.002	0.070
NM_001082839	*wdr85*	WD repeat domain 85	1.72	0.002	0.067
NM_199992	*sema6a*	sema domain, transmembrane domain (TM), and cytoplasmic domain, (semaphorin) 6A	1.72	0.019	0.271
NM_001177744	*aqp9b*	aquaporin 9b	1.70	0.005	0.131
NM_001002512	zgc:92818	zgc:92818	1.70	0.008	0.187
NM_199674	*stub1*	STIP1 homology and U-Box containing protein 1	1.69	0.031	0.332
NM_001103125	*fam46a*	family with sequence similarity 46, member A	1.69	0.011	0.211
NM_001033091	si:ch211-237l4.6	si:ch211-237l4.6	1.69	0.003	0.109
NM_001020663	*bach1*	BTB and CNC homology 1, basic leucine zipper transcription factor 1	1.68	0.019	0.269
NM_200179	*cdc14b*	CDC14 cell division cycle 14 homolog B	1.68	0.003	0.096
NM_001167826	zgc:73329	zgc:73329	1.68	0.028	0.314
NM_200989	*pacsin3*	protein kinase C and casein kinase substrate in neurons 3	1.68	0.008	0.181
NM_001002722	*ttc33*	tetratricopeptide repeat domain 33	1.67	0.018	0.267
NM_001003493	*suds3*	suppressor of defective silencing 3 homolog (SDS3, S. cerevisiae)	1.67	0.035	0.349
NM_001007778	*gpsm1b*	G-protein signaling modulator 1b	1.66	0.037	0.353
NM_001003479	*rasgef1bb*	RasGEF domain family, member 1Bb	1.66	0.020	0.278
NM_201153	*rps3*	ribosomal protein S3	1.66	0.004	0.128
NM_199777	*sec23b*	Sec23 homolog B (S. cerevisiae)	1.66	0.017	0.265
NM_130968	*odz3*	odd Oz/ten-m homolog 3	1.66	0.007	0.165
NM_213415	*zbtb2b*	zinc finger and BTB domain containing 2b	1.66	0.021	0.281
NM_201315	*abcf2a*	ATP-binding cassette, sub-family F (GCN20), member 2a	1.65	0.005	0.137
NM_200724	*guk1b*	guanylate kinase 1b	1.65	0.002	0.075

Genbank accession number	Gene symbol	Gene description	fold change	P value	Q value
NM_198363	*tob1a*	transducer of ERBB2, 1a	1.64	0.003	0.101
NM_001080036	*tp53inp1*	tumor protein p53 inducible nuclear protein 1	1.64	0.014	0.240
NM_001256204	*elac2*	elaC homolog 2 (E. coli)	1.64	0.032	0.334
NM_001030234	zgc:113372	zgc:113372	1.64	0.045	0.381
NM_001045485	*pi4k2b*	phosphatidylinositol 4-kinase type 2 beta	1.64	0.005	0.131
NM_212645	*hnrnpa0a*	heterogeneous nuclear ribonucleoprotein A0a	1.63	0.003	0.101
NM_200949	*zfand5b*	zinc finger, AN1-type domain 5b	1.63	0.010	0.199
NM_199215	*ca2*	carbonic anhydrase II	1.63	0.002	0.066
NM_001002355	zgc:92139	zgc:92139	1.63	0.008	0.182
NM_001077379	*sec23ip*	SEC23 interacting protein	1.63	0.021	0.280
NM_001126454	*fam222a*	family with sequence similarity 222, member A	1.62	0.041	0.370
NM_001002708	*pde6d*	phosphodiesterase 6D, cGMP-specific, rod, delta	1.62	0.002	0.072
NM_200276	*ncor1*	nuclear receptor co-repressor 1	1.62	0.003	0.088
NM_001006016	*atl3*	atlastin 3	1.62	0.046	0.382
NM_001110123	*oscp1a*	organic solute carrier partner 1a	1.62	0.002	0.066
NM_001082998	*fosl2*	fos-like antigen 2	1.62	0.012	0.222
NM_001044859	si:ch211-15d5.5	si:ch211-15d5.5	1.62	0.029	0.318
NM_001044848	*arhgef1b*	Rho guanine nucleotide exchange factor (GEF) 1b	1.61	0.020	0.273
NM_212963	*dip2ba*	DIP2 disco-interacting protein 2 homolog Ba (Drosophila)	1.61	0.007	0.163
NM_001080651	*creb3l2*	cAMP responsive element binding protein 3-like 2	1.61	0.007	0.163
NM_131081	*cdh2*	cadherin 2, neuronal	1.61	0.013	0.232
NM_213198	*orc5*	origin recognition complex, subunit 5	1.61	0.002	0.079
NM_001077768	*zranb1b*	zinc finger, RAN-binding domain containing 1b	1.61	0.012	0.228

Genbank accession number	Gene symbol	Gene description	fold change	P value	Q value
NM_001128534	*arvcfb*	armadillo repeat gene deleted in velocardiofacial syndrome b	1.60	0.004	0.116
NM_213497	*crip2*	cysteine-rich protein 2	1.60	0.011	0.216
NM_212684	*atxn2l*	ataxin 2-like	1.60	0.020	0.276
NM_001130663	si:ch211-160i2.3	si:ch211-160i2.3	1.59	0.048	0.385
NM_199830	*klhl18*	kelch-like 18 (Drosophila)	1.58	0.015	0.248
NM_001002495	*uqcrq*	ubiquinol-cytochrome c reductase, complex III subunit VII	1.58	0.043	0.375
NM_001017800	zgc:110331	zgc:110331	1.58	0.003	0.102
NM_200813	*ca7*	carbonic anhydrase VII	1.58	0.028	0.314
NM_001128259	*uckl1a*	uridine-cytidine kinase 1-like 1a	1.58	0.004	0.124
NM_199480	*lnpa*	limb and neural patterns a	1.58	0.019	0.269
NM_001165918	wu:fb15g10	wu:fb15g10	1.58	0.023	0.293
NM_001083075	*znf865*	zinc finger protein 865	1.57	0.012	0.219
NM_199541	*id2b*	inhibitor of DNA binding 2, dominant negative helix-loop-helix protein, b	1.57	0.019	0.269
NM_001044786	*shoc2*	soc-2 suppressor of clear homolog (C. elegans)	1.57	0.018	0.267
NM_001170739	*mga*	MAX gene associated	1.57	0.005	0.139
NM_212974	*tob1b*	transducer of ERBB2, 1b	1.56	0.003	0.091
NM_212955	esrra	estrogen-related receptor alpha	1.56	0.041	0.370
NM_001034976	*prkacbb*	protein kinase, cAMP-dependent, catalytic, beta b	1.56	0.032	0.336
NM_001044918	*znf704*	zinc finger protein 704	1.56	0.026	0.306
NM_001144784	*inaa*	internexin neuronal intermediate filament protein, alpha a	1.55	0.003	0.109
NM_201470	*ip6k2*	inositol hexaphosphate kinase 2	1.55	0.015	0.251
NM_194380	*dusp6*	dual specificity phosphatase 6	1.55	0.004	0.112
NM_001127515	si:dkey-110k5.6	si:dkey-110k5.6	1.55	0.018	0.267

Genbank accession number	Gene symbol	Gene description	fold change	P value	Q value
NM_131900	*cacna1c*	calcium channel, voltage-dependent, L type, alpha 1C subunit	1.55	0.009	0.198
NM_201149	*cdc14aa*	CDC14 cell division cycle 14 homolog A, a	1.54	0.010	0.206
NM_200064	*bcat1*	branched chain aminotransferase 1, cytosolic	1.54	0.012	0.222
NM_001012378	*dlg2*	discs, large (Drosophila) homolog 2	1.54	0.027	0.312
NM_213149	*fkbp5*	FK506 binding protein 5	1.54	0.037	0.353
NM_212759	*cyfip1*	cytoplasmic FMR1 interacting protein 1	1.53	0.009	0.198
NM_001159971	*spty2d1*	SPT2, Suppressor of Ty, domain containing 1 (S. cerevisiae)	1.53	0.019	0.269
NM_001098177	*myh9a*	myosin, heavy polypeptide 9a, non-muscle	1.53	0.005	0.144
NM_001110279	*mll*	myeloid/lymphoid or mixed-lineage leukemia (trithorax homolog, Drosophila)	1.53	0.011	0.210
NM_001007330	*cbl*	Cas-Br-M (murine) ecotropic retroviral transforming sequence	1.53	0.042	0.374
NM_194399	*cflar*	CASP8 and FADD-like apoptosis regulator	1.52	0.028	0.318
NM_001145089	*camk2n1a*	calcium/calmodulin-dependent protein kinase II inhibitor 1a	1.52	0.016	0.256
NM_001030136	*daam1b*	dishevelled associated activator of morphogenesis 1b	1.52	0.016	0.261
NM_001001940	*copb2*	coatomer protein complex, subunit beta 2	1.52	0.020	0.276
NM_212732	*mdm4*	transformed 3T3 cell double minute 4 homolog (mouse)	1.51	0.048	0.385
NM_001012304	*rbm39a*	RNA binding motif protein 39a	1.51	0.007	0.168
NM_001044911	*nrg1*	neuregulin 1	1.51	0.012	0.222
NM_001007032	*ncor2*	nuclear receptor co-repressor 2	1.51	0.042	0.371
NM_213442	*srrm1*	serine/arginine repetitive matrix 1	1.50	0.044	0.380
NM_001089366	*morc3a*	MORC family CW-type zinc finger 3a	1.50	0.048	0.385
NM_200595	*fbxo45*	F-box protein 45	1.50	0.046	0.382
NM_001114926	*c3orf58b*	C3orf58 chromosome 3 open reading frame 58, b	1.49	0.019	0.269
NM_199672	*stk3*	serine/threonine kinase 3 (STE20 homolog, yeast)	1.49	0.033	0.341

Genbank accession number	Gene symbol	Gene description	fold change	P value	Q value
NM_001020660	*cyb5r4*	cytochrome b5 reductase 4	1.49	0.023	0.293
NM_001004553	*ppp3r1b*	protein phosphatase 3 (formerly 2B), regulatory s1ubunit B, alpha isoform, b	1.49	0.010	0.201
NM_131183	*nr2f2*	nuclear receptor subfamily 2, group F, member 2	1.48	0.026	0.308
NM_213489	*prpf38b*	PRP38 pre-mRNA processing factor 38 (yeast) domain containing B	1.48	0.043	0.374
NM_131411	*aanat2*	arylalkylamine N-acetyltransferase	1.48	0.012	0.219
NM_194362	*ube4b*	ubiquitination factor E4B, UFD2 homolog (S. cerevisiae)	1.48	0.018	0.267
NM_194427	*slc7a4*	solute carrier family 7 (cationic amino acid transporter, y+ system), member 4	1.48	0.046	0.382
NM_001002681	zgc:86841	zgc:86841	1.47	0.045	0.382
NM_001024440	*spc24*	SPC24, NDC80 kinetochore complex component, homolog (S. cerevisiae)	1.47	0.044	0.379
NM_001246660	*rpgrip1l*	RPGRIP1-like	1.47	0.048	0.385
NM_001197074	*u2surp*	U2 snRNP-associated SURP domain containing	1.47	0.022	0.284
NM_001110371	*ppp4r2b*	protein phosphatase 4, regulatory subunit 2b	1.47	0.042	0.372
NM_001044914	*trim8*	tripartite motif-containing 8	1.47	0.031	0.328
NM_213379	*got2a*	glutamic-oxaloacetic transaminase 2a, mitochondrial (aspartate aminotransferase 2)	1.46	0.014	0.245
NM_001082840	*prkacaa*	protein kinase, cAMP-dependent, catalytic, alpha, genome duplicate a	1.46	0.037	0.353
NM_001089401	*ubtd1a*	ubiquitin domain containing 1a	1.46	0.030	0.325
NM_131406	*raraa*	retinoic acid receptor, alpha a	1.46	0.047	0.382
NM_199273	zgc:66433	zgc:66433	1.45	0.012	0.228
NM_001045073	*hsp90aa1.2*	heat shock protein 90, alpha (cytosolic), class A member 1, tandem duplicate 2	1.45	0.020	0.278
NM_200697	*ckmt2*	creatine kinase, mitochondrial 2 (sarcomeric)	1.45	0.032	0.336
NM_131031	*actb1*	actin, beta 1	1.45	0.027	0.313
NM_001029966	*trnau1apl*	tRNA selenocysteine 1 associated protein 1, like	1.44	0.041	0.370
NM_173274	*dag1*	dystroglycan 1	1.44	0.035	0.349

Genbank accession number	Gene symbol	Gene description	fold change	P value	Q value
NM_001007152	*dpf2*	D4, zinc and double PHD fingers family 2	1.44	0.046	0.382
NM_001030116	*scrn2*	secernin 2	1.44	0.036	0.351
NM_200472	*pygmb*	phosphorylase, glycogen (muscle) b	1.44	0.020	0.275
NM_001044982	*cited4a*	Cbp/p300-interacting transactivator, with Glu/Asp-rich carboxy-terminal domain, 4a	1.44	0.029	0.322
NM_200867	*srsf5a*	serine/arginine-rich splicing factor 5a	1.44	0.044	0.377
NM_212644	*dennd5b*	DENN/MADD domain containing 5B	1.44	0.026	0.308
NM_001045108	*fam65a*	family with sequence similarity 65, member A	1.43	0.034	0.345
NM_001128539	*zbtb10*	zinc finger and BTB domain containing 10	1.43	0.025	0.304
NM_199983	*mylipa*	myosin regulatory light chain interacting protein a	1.43	0.028	0.314
NM_131015	*mafba*	glutamate receptor, ionotropic, N-methyl D-aspartate 1b	1.43	0.026	0.309
NM_001017618	*icmt*	isoprenylcysteine carboxyl methyltransferase	1.42	0.031	0.332
NM_001045049	si:ch211-69g19.2	si:ch211-69g19.2	1.42	0.050	0.388
NM_212749	*rhoab*	ras homolog gene family, member Ab	1.42	0.038	0.356
NM_199333	*pkma*	pyruvate kinase, muscle, a	1.42	0.028	0.318
NM_001007287	*fhla*	four and a half LIM domains a	1.42	0.027	0.314
NM_001089363	*ccnl1a*	cyclin L1a	1.41	0.040	0.365
NM_213397	*pfkfb3*	6-phosphofructo-2-kinase/fructose-2,6-biphosphatase 3	1.41	0.046	0.382
NM_001003612	*boka*	BCL2-related ovarian killer a	1.40	0.026	0.308
NM_001004552	*pdxdc1*	pyridoxal-dependent decarboxylase domain containing 1	1.40	0.027	0.313
NM_213333	*sltm*	SAFB-like, transcription modulator	1.39	0.034	0.344
NM_200704	*aanat1*	arylalkylamine N-acetyltransferase 1	1.39	0.042	0.373
NM_001044993	*nfs1*	NFS1 nitrogen fixation 1 (S. cerevisiae)	1.38	0.041	0.370
NM_207072	*clasp2*	cytoplasmic linker associated protein 2	1.38	0.041	0.369

Genbank accession number	Gene symbol	Gene description	fold change	P value	Q value
NM_001007295	zgc:92107	zgc:92107	1.36	0.039	0.361
NM_001005402	*cdhr1a*	cadherin-related family member 1a	1.36	0.041	0.370
NM_205762	*traf4a*	tnf receptor-associated factor 4a	1.36	0.049	0.386
NM_200150	*ankrd12*	ankyrin repeat domain 12	1.36	0.045	0.382
NM_001123253	LOC560226	novel protein similar to vertebrate breakpoint cluster region (BCR)	1.35	0.044	0.377

Values were calculated with Cuffdiff, n=3.

Q-values represent adjusted P values with Benjemini and Hochberg procedure for multiple testing.

Down-regulated genes in the ES1-expressing rods. Genes were sorted in ascending order according to the value of fold change.

Genbank accession number	Gene symbol	Gene description	fold change	P value	Q value
NM_001256251	*msnb*	moesin b	0.08	5.0E-5	0.005
NM_001003987	*epb41l3a*	erythrocyte membrane protein band 4.1-like 3a	0.16	2.5E-4	0.017
NM_001168350	*adcy1b*	adenylate cyclase 1b	0.17	0.015	0.249
NM_001128759	zgc:194989	zgc:194989	0.20	0.002	0.066
NM_001076593	zgc:153394	zgc:153394	0.20	0.003	0.097
NM_001017846	*rgs16*	regulator of G-protein signaling 16	0.21	0.006	0.151
NM_001003629	*rgs3*	regulator of G-protein signaling 3	0.21	4.5E-4	0.026
NM_001004671	*uxt*	ubiquitously-expressed transcript	0.26	0.012	0.226
NM_212680	*hmga2*	high mobility group AT-hook 2	0.29	5.0E-5	0.005
NM_213398	*vamp1*	vesicle-associated membrane protein 1	0.30	0.042	0.372
NM_131098	*apoeb*	apolipoprotein Eb	0.30	5.0E-5	0.005
NM_001025464	*pdcb*	phosducin b	0.31	5.0E-5	0.005
NM_001113589	*hsp70l*	heat shock cognate 70-kd protein, like	0.32	5.0E-5	0.005
NM_001045173	*ndrg4*	N-myc downstream regulated gene 4	0.33	5.0E-5	0.005
NM_001005924	*tmem56b*	transmembrane protein 56b	0.34	5.0E-5	0.005
NM_200199	*smu1*	smu-1 suppressor of mec-8 and unc-52 homolog (C. elegans)	0.35	2.5E-4	0.017
NR_029934	*mir204-1*	microRNA 204-1	0.35	3.0E-4	0.019
NM_131397	*hsp70*	heat shock cognate 70-kd protein	0.35	5.0E-5	0.005
NM_001007351	*btg3*	B-cell translocation gene 3	0.35	0.007	0.170
NM_001020550	*tp53rk*	TP53 regulating kinase	0.36	0.003	0.108
NM_200455	zgc:63568	zgc:63568	0.37	0.013	0.236

Genbank accession number	Gene symbol	Gene description	fold change	P value	Q value
NM_001083843	*comtb*	catechol-O-methyltransferase b	0.37	5.0E-5	0.005
NM_001045138	*pdcd2*	programmed cell death 2	0.38	0.012	0.223
NM_001034968	*slit1a*	slit homolog 1a (Drosophila)	0.38	5.0E-5	0.005
NM_001007282	*gpx4a*	glutathione peroxidase 4a	0.38	1.0E-4	0.008
NM_201093	*tnni2a.2*	troponin I, skeletal, fast 2a.2	0.38	3.0E-4	0.019
NM_199569	*eif2s1l*	eukaryotic translation initiation factor 2, subunit 1 alpha, like	0.38	0.007	0.163
NM_001080020	*grma*	glutamate receptor, metabotropic a	0.38	5.0E-5	0.005
NM_001089391	*slc5a5*	solute carrier family 5 (sodium iodide symporter), member 5	0.39	2.5E-4	0.017
NM_001076667	*dync1i2a*	dynein, cytoplasmic 1, intermediate chain 2a	0.40	0.048	0.385
NM_152961	*fabp3*	fatty acid binding protein 3, muscle and heart	0.40	5.5E-4	0.030
NM_001144131	*grin1b*	glutamate receptor, ionotropic, N-methyl D-aspartate 1b	0.40	1.0E-4	0.008
NM_131869	*gnat2*	guanine nucleotide binding protein (G protein), alpha transducing activity polypeptide 2	0.41	5.0E-5	0.005
NM_001006093	*scp2b*	sterol carrier protein 2b	0.41	9.0E-4	0.044
NM_001002875	*gnl3l*	guanine nucleotide binding protein-like 3 (nucleolar)-like	0.41	0.010	0.200
NM_131055	*flh*	floating head	0.41	0.001	0.051
NM_213373	*znf330*	zinc finger protein 330	0.43	0.018	0.267
NM_001003516	zgc:100908	zgc:100908	0.43	0.041	0.371
NM_200871	*pde6c*	phosphodiesterase 6C, cGMP-specific, cone, alpha prime	0.43	2.0E-4	0.015
NM_200698	*cabp5a*	calcium binding protein 5a	0.43	0.003	0.108
NM_173284	*tsr2*	TSR2, 20S rRNA accumulation, homolog (S. cerevisiae)	0.44	0.026	0.306
NM_131070	*mdka*	midkine-related growth factor	0.44	0.005	0.138
NM_201072	*rtn3*	reticulon 3	0.44	5.5E-4	0.030
NM_205645	*pigf*	phosphatidylinositol glycan, class F	0.45	0.022	0.287

Genbank accession number	Gene symbol	Gene description	fold change	P value	Q value
NM_001089466	*srebf2*	sterol regulatory element binding transcription factor 2	0.45	5.0E-5	0.005
NM_001004529	*echs1*	enoyl Coenzyme A hydratase, short chain, 1, mitochondrial	0.45	0.001	0.062
NM_001007329	*slc7a3a*	solute carrier family 7 (cationic amino acid transporter, y+ system), member 3a	0.45	5.0E-5	0.005
NM_201059	*waslb*	Wiskott-Aldrich syndrome-like b	0.46	3.5E-4	0.021
NM_001045078	zk13a21.14	coiled-coil domain containing 120-like	0.46	0.003	0.098
NM_001130612	*atxn10*	ataxin 10	0.46	0.019	0.272
NM_001037112	zgc:123238	zgc:123238	0.46	0.007	0.163
NM_198374	*pik3ip1*	phosphoinositide-3-kinase interacting protein 1	0.46	0.003	0.098
NM_205653	*znf410*	zinc finger protein 410	0.46	0.009	0.189
NM_200837	zgc:73359	zgc:73359	0.46	0.033	0.340
NM_001115051	si:dkey-5i22.6	si:dkey-5i22.6	0.47	0.006	0.150
NM_001020696	*alg3*	asparagine-linked glycosylation 3 homolog (S. cerevisiae, alpha-1,3-mannosyltransferase)	0.47	0.018	0.267
NM_001033749	*sagb*	S-antigen; retina and pineal gland (arrestin) b	0.47	0.008	0.176
NM_198357	*tcerg1a*	transcription elongation regulator 1a (CA150)	0.48	5.0E-5	0.005
NM_001144792	*cept1a*	choline/ethanolamine phosphotransferase 1a	0.48	0.003	0.109
NM_200692	*ndrg1b*	N-myc downstream regulated gene 1b	0.48	0.006	0.153
NM_001077611	*dars*	aspartyl-tRNA synthetase	0.48	0.005	0.137
NM_001002094	*msrb3*	methionine sulfoxide reductase B3	0.48	0.006	0.154
NM_001025502	*h2afy2*	H2A histone family, member Y2	0.48	0.008	0.182
NM_001044856	*ociad2*	OCIA domain containing 2	0.48	2.5E-4	0.017
NM_001037239	zgc:123177	zgc:123177	0.48	0.017	0.265
NM_153666	*tbx24*	T-box 24	0.48	0.006	0.146
NM_001030251	zgc:114103	zgc:114103	0.49	3.5E-4	0.021

Genbank accession number	Gene symbol	Gene description	fold change	P value	Q value
NM_200095	*asnsd1*	asparagine synthetase domain containing 1	0.49	0.025	0.303
NM_198070	*tkt*	transketolase	0.49	3.0E-4	0.019
NM_001105129	*srebf1*	sterol regulatory element binding transcription factor 1	0.49	5.0E-5	0.005
NM_200783	*efna1b*	ephrin A1b	0.49	0.018	0.267
NM_001005601	*tmem18*	transmembrane protein 18	0.49	0.008	0.176
NM_001039808	*slc2a1a*	solute carrier family 2 (facilitated glucose transporter), member 1a	0.50	9.0E-4	0.044
NM_001032366	*dcun1d4*	DCN1, defective in cullin neddylation 1, domain containing 4 (S. cerevisiae)	0.50	5.0E-5	0.005
NM_213126	*b2ml*	beta-2-microglobulin, like	0.50	5.0E-5	0.005
NM_199529	*mthfd1b*	methylenetetrahydrofolate dehydrogenase (NADP+ dependent) 1b	0.50	0.002	0.066
NM_131397	*hsp70*	heat shock cognate 70-kd protein	0.51	5.0E-5	0.005
NM_213205	*m6pr*	mannose-6-phosphate receptor (cation dependent)	0.51	0.018	0.267
NM_001145564	*cyp2u1*	cytochrome P450, family 2, subfamily U, polypeptide 1	0.52	0.015	0.251
NM_199727	*serinc1*	serine incorporator 1	0.52	5.0E-5	0.005
NM_205700	*cfl2*	cofilin 2 (muscle)	0.52	0.009	0.198
NM_001003566	*phpt1*	phosphohistidine phosphatase 1	0.52	0.009	0.198
NM_001045293	*flj11011l*	hypothetical protein FLJ11011-like (H. sapiens)	0.52	0.006	0.163
NM_001004530	*fuom*	fucose mutarotase	0.52	0.039	0.364
NM_001126485	LOC100006564	novel NACHT domain containing protein	0.53	0.020	0.274
NM_199745	*esf1*	ESF1, nucleolar pre-rRNA processing protein, homolog (S. cerevisiae)	0.53	0.022	0.283
NM_213202	*gnb3b*	guanine nucleotide binding protein (G protein), beta polypeptide 3b	0.53	0.001	0.062
NM_001076569	zgc:153980	zgc:153980	0.53	0.002	0.076
NM_213527	*hiat1b*	hippocampus abundant transcript 1b	0.53	0.003	0.087
NM_213104	*pgrmc2*	progesterone receptor membrane component 2	0.53	0.006	0.156

Genbank accession number	Gene symbol	Gene description	fold change	P value	Q value
NM_201464	*impdh2*	IMP (inosine monophosphate) dehydrogenase 2	0.54	0.025	0.303
NM_131205	*etv5b*	ets variant 5b	0.54	0.006	0.155
NM_198368	*taf12*	TAF12 RNA polymerase II, TATA box binding protein (TBP)-associated factor	0.54	0.018	0.267
NM_001020733	*lin7b*	lin-7 homolog B (C. elegans)	0.54	0.025	0.301
NM_178297	*sepp1a*	selenoprotein P, plasma, 1a	0.54	0.002	0.064
NM_001171587	*prox1b*	prospero-related homeobox gene 1b	0.54	0.008	0.176
NM_001115122	*dpp6b*	dipeptidyl-peptidase 6b	0.55	0.002	0.082
NM_200745	*edf1*	endothelial differentiation-related factor 1	0.55	0.026	0.308
NM_205570	zgc:73226	zgc:73226	0.55	2.5E-4	0.017
NM_205759	*eepd1*	endonuclease/exonuclease/phosphatase family domain containing 1	0.55	0.032	0.336
NM_001034988	*cx41.8*	connexin 41.8	0.55	0.018	0.267
NM_001089338	zgc:162958	zgc:162958	0.55	0.010	0.208
NM_001007422	zgc:100824	zgc:100824	0.56	0.038	0.356
NM_001023581	*tmem167a*	transmembrane protein 167A	0.56	0.021	0.281
NM_001014313	*tmem35*	transmembrane protein 35	0.56	0.005	0.131
NM_001114702	zgc:174710	zgc:174710	0.56	1.1E-3	0.050
NM_001083544	*rbx1*	ring-box 1	0.56	0.010	0.207
NM_001190382	*sell*	selenoprotein L	0.57	0.040	0.365
NM_131400	*tefa*	thyrotroph embryonic factor a	0.57	0.002	0.066
NM_212629	*ubr7*	ubiquitin protein ligase E3 component n-recognin 7	0.57	0.007	0.163
NM_199582	*tpd52l2b*	tumor protein D52-like 2b	0.57	0.046	0.382
NM_199869	*insig1*	insulin induced gene 1	0.57	0.041	0.370
NM_001005990	*kansl2*	KAT8 regulatory NSL complex subunit 2	0.57	0.043	0.375

Genbank accession number	Gene symbol	Gene description	fold change	P value	Q value
NM_152886	*appb*	amyloid beta (A4) precursor protein b	0.58	4.0E-4	0.024
NM_212990	*eif3i*	eukaryotic translation initiation factor 3, subunit I	0.58	0.036	0.352
NM_001039981	zgc:136866	zgc:136866	0.58	0.047	0.382
NM_001007291	*oxct1a*	3-oxoacid CoA transferase 1a	0.58	0.030	0.325
NM_001082997	*si:dkey-23c22.6*	si:dkey-23c22.6	0.58	0.003	0.097
NM_001004648	*nudt4b*	nudix (nucleoside diphosphate linked moiety X)-type motif 4b	0.58	0.018	0.267
NM_200766	*paip2b*	poly(A) binding protein interacting protein 2B	0.58	0.011	0.218
NM_001020775	zgc:113201	zgc:113201	0.59	0.050	0.389
NM_001077391	zgc:153997	zgc:153997	0.59	0.002	0.084
NM_001089335	*bri3bp*	bri3 binding protein	0.59	0.023	0.290
NM_001002634	*nipal3*	NIPA-like domain containing 3	0.59	0.028	0.314
NM_199793	*dazap2*	DAZ associated protein 2	0.59	0.003	0.095
NM_001006087	*ormdl3*	ORM1-like 3 (S. cerevisiae)	0.59	0.007	0.163
NM_199481	*ccng1*	cyclin G1	0.59	0.009	0.196
NM_212575	*mtx2*	metaxin 2	0.59	0.035	0.346
NM_001079969	*spoplb*	speckle-type POZ protein-like b	0.60	0.040	0.365
NM_201036	*vti1b*	vesicle transport through interaction with t-SNAREs homolog 1B (yeast)	0.60	0.027	0.312
NM_001002707	zgc:92606	zgc:92606	0.60	0.005	0.139
NM_001004605	*arrdc3b*	arrestin domain containing 3b	0.60	0.006	0.156
NM_201067	*rorab*	RAR-related orphan receptor A, paralog b	0.60	0.010	0.203
NM_214819	*rcan2*	regulator of calcineurin 2	0.60	0.017	0.265
NM_001020714	zgc:113162	zgc:113162	0.60	0.048	0.385
NM_198978	*pdcd4b*	programmed cell death 4b	0.60	0.004	0.120

Genbank accession number	Gene symbol	Gene description	fold change	P value	Q value
NM_214770	*rab11ba*	RAB11B, member RAS oncogene family, a	0.60	0.038	0.356
NM_001005932	*tars*	threonyl-tRNA synthetase	0.60	0.030	0.325
NM_001080079	*mapkapk3*	mitogen-activated protein kinase-activated protein kinase 3	0.60	0.015	0.249
NM_001024221	*wdr33*	WD repeat domain 33	0.60	0.045	0.381
NM_001045564	*psmb7*	proteasome (prosome, macropain) subunit, beta type, 7	0.60	0.039	0.364
NM_213407	*zranb2*	zinc finger, RAN-binding domain containing 2	0.61	0.006	0.146
NM_001014306	*lifra*	leukemia inhibitory factor receptor alpha a	0.61	0.009	0.196
NM_199681	*phb2*	prohibitin 2	0.61	0.015	0.251
NM_212708	*slc16a3*	solute carrier family 16 (monocarboxylic acid transporters), member 3	0.61	0.006	0.156
NM_001017732	*prkar1ab*	protein kinase, cAMP-dependent, regulatory, type I, alpha (tissue specific extinguisher 1) b	0.61	0.007	0.163
NM_212850	*glcea*	glucuronyl C5-epimerase a	0.61	0.022	0.283
NM_001003875	*snrnp70*	small nuclear ribonucleoprotein 70 (U1)	0.61	0.002	0.066
NM_205745	*wdfy2*	WD repeat and FYVE domain containing 2	0.61	0.046	0.382
NM_201171	*dusp4*	dual specificity phosphatase 4	0.62	0.008	0.176
NM_131065	*nr1d2b*	nuclear receptor subfamily 1, group D, member 2b	0.62	0.025	0.304
NM_201111	*hook2*	hook homolog 2 (Drosophila)	0.62	0.009	0.196
NM_001044840	*tmem181*	transmembrane protein 181	0.62	0.024	0.297
NM_001029968	*nif3l1*	NIF3 NGG1 interacting factor 3-like 1 (S. cerevisiae)	0.62	0.037	0.353
NM_001025538	*tspan3a*	tetraspanin 3a	0.62	0.002	0.069
NM_001256646	*flrt3*	fibronectin leucine rich transmembrane 3	0.62	0.010	0.209
NM_001080074	zgc:158316	zgc:158316	0.62	0.027	0.312
NM_213435	zgc:55683	zgc:55683	0.63	0.033	0.337
NM_131758	*stom*	stomatin	0.63	0.005	0.137

Genbank accession number	Gene symbol	Gene description	fold change	P value	Q value
NM_001013312	zgc:113324	zgc:113324	0.63	0.042	0.374
NM_001128811	zgc:194176	zgc:194176	0.63	0.024	0.300
NM_001201344	*slc43a3a*	solute carrier family 43, member 3a	0.63	0.007	0.163
NM_212904	*chmp2bb*	chromatin modifying protein 2Bb	0.63	0.046	0.382
NM_001110479	*trpm1b*	transient receptor potential cation channel, subfamily M, member 1b	0.63	0.021	0.281
NM_001089562	*rab8a*	RAB8A, member RAS oncogene family	0.63	0.020	0.278
NM_001089384	zgc:162698	zgc:162698	0.63	0.009	0.191
NM_001003731	zgc:91910	zgc:91910	0.63	0.048	0.385
NM_001045295	*farsa*	phenylalanyl-tRNA synthetase, alpha subunit	0.64	0.047	0.382
NM_213308	*stk25b*	serine/threonine kinase 25b	0.64	0.019	0.269
NM_001007424	*dhrs13a.3*	dehydrogenase/reductase (SDR family) member 13a.3	0.64	0.032	0.336
NM_001003623	*naa50*	N(alpha)-acetyltransferase 50, NatE catalytic subunit	0.64	0.039	0.361
NM_001044942	*parp1*	poly (ADP-ribose) polymerase family, member 1	0.64	0.027	0.312
NM_199919	*ap2b1*	adaptor-related protein complex 2, beta 1 subunit	0.65	0.013	0.234
NM_213262	*eif5a2*	eukaryotic translation initiation factor 5A2	0.65	0.008	0.174
NM_001079977	*hmgcra*	3-hydroxy-3-methylglutaryl-Coenzyme A reductase a	0.65	0.009	0.191
NM_182967	*calm3a*	calmodulin 3a (phosphorylase kinase, delta)	0.65	0.014	0.244
NM_001008617	*ttc26*	tetratricopeptide repeat domain 26	0.65	0.040	0.369
NM_213087	*sdf4*	stromal cell derived factor 4	0.65	0.013	0.228
NM_201327	*ssr1*	signal sequence receptor, alpha	0.65	0.030	0.328
NM_001170599	*tbx21*	T-box 21	0.65	0.030	0.328
NM_001037699	*golph3l*	golgi phosphoprotein 3-like	0.65	0.048	0.385
NM_199555	*hmgb1a*	high-mobility group box 1a	0.65	0.011	0.214

Genbank accession number	Gene symbol	Gene description	fold change	P value	Q value
NM_001003861	*rpl9*	ribosomal protein L9	0.66	0.017	0.264
NM_131451	*irbp*	interphotoreceptor retinoid-binding protein	0.66	0.030	0.325
NM_199965	*rbp4l*	retinol binding protein 4, like	0.66	0.019	0.271
NM_001040313	zgc:136739	zgc:136739	0.66	0.017	0.266
NM_001082872	*nat15*	N-acetyltransferase 15 (GCN5-related, putative)	0.66	0.048	0.385
NM_001076663	*rabggta*	Rab geranylgeranyltransferase, alpha subunit	0.66	0.045	0.381
NM_001128358	LOC797250	novel protein similar to H.sapiens solute carrier family 7 (cationic amino acid transporter, y+ system), member 5	0.66	0.011	0.216
NM_001083002	*arid3b*	AT rich interactive domain 3B (Bright like)	0.66	0.012	0.219
NM_001030102	*brms1la*	breast cancer metastasis-suppressor 1-like a	0.67	0.040	0.365
NM_001103111	*mntb*	MAX binding protein b	0.67	0.027	0.312
NM_194417	*sepw2a*	selenoprotein W, 2a	0.67	0.011	0.215
NM_213529	*tmem50a*	transmembrane protein 50A	0.67	0.040	0.367
NM_001045402	*cbx3a*	chromobox homolog 3a (HP1 gamma homolog, Drosophila)	0.67	0.048	0.385
NM_001114585	zgc:174944	zgc:174944	0.67	0.020	0.274
NM_173254	*atp6v1e1b*	ATPase, H+ transporting, lysosomal, V1 subunit E isoform 1b	0.67	0.015	0.251
NM_001013337	zgc:113200	zgc:113200	0.67	0.029	0.319
NM_001045052	*tmem106bb*	transmembrane protein 106Bb	0.67	0.013	0.231
NM_131710	*ctsd*	cathepsin D	0.68	0.024	0.296
NM_001130192	*pnrc2*	proline-rich nuclear receptor coactivator 2	0.68	0.020	0.273
NM_212912	*tmed7*	transmembrane emp24 protein transport domain containing 7	0.68	0.029	0.319
NM_001077376	si:ch211-133n4.4	si:ch211-133n4.4	0.68	0.023	0.290
NM_131465	*pcmt*	l-isoaspartyl protein carboxyl methyltransferase	0.69	0.023	0.291
NM_001002353	*dnajb6a*	DnaJ (Hsp40) homolog, subfamily B, member 6a	0.69	0.045	0.381

Genbank accession number	Gene symbol	Gene description	fold change	P value	Q value
NM_001077568	*ctsf*	cathepsin F	0.69	0.016	0.256
NM_201166	*dctn2*	dynactin 2 (p50)	0.69	0.037	0.356
NM_178306	*tph1a*	tryptophan hydroxylase 1 (tryptophan 5-monooxygenase) a	0.69	0.028	0.314
NM_200009	*eef1a1a*	eukaryotic translation elongation factor 1 alpha 1a	0.69	0.015	0.248
NM_199666	*ndfip1*	Nedd4 family interacting protein 1	0.70	0.019	0.271
NM_200362	*tmem106ba*	transmembrane protein 106Ba	0.70	0.029	0.320
NM_001025475	*idi1*	isopentenyl-diphosphate delta isomerase 1	0.70	0.041	0.371
NM_001099448	*wwp2*	WW domain containing E3 ubiquitin protein ligase 2	0.70	0.048	0.385
NM_001144040	*cog3*	component of oligomeric golgi complex 3	0.70	0.038	0.356
NM_199957	*ppiab*	peptidylprolyl isomerase Ab (cyclophilin A)	0.70	0.050	0.389
NM_001167570	*pvrl1a*	poliovirus receptor-related 1a	0.70	0.050	0.389
NM_200925	*stau2*	staufen, RNA binding protein, homolog 2 (Drosophila)	0.71	0.035	0.350
NM_201112	*arl6ip1*	ADP-ribosylation factor-like 6 interacting protein 1	0.71	0.031	0.332
NM_178290	*selt1a*	selenoprotein T, 1a	0.71	0.034	0.346
NM_001164027	*npepps*	aminopeptidase puromycin sensitive	0.71	0.037	0.356
NM_001252649	si:ch211-117m20.5	si:ch211-117m20.5	0.72	0.037	0.353
NM_213250	*csnk1db*	casein kinase 1, delta b	0.73	0.048	0.385
NM_199587	*lztfl1*	leucine zipper transcription factor-like 1	0.73	0.049	0.387
NM_001002298	*asna1*	arsA arsenite transporter, ATP-binding, homolog 1 (bacterial)	0.73	0.046	0.382

Values were calculated with Cuffdiff, n=3.

Q-values represent adjusted P values with Benjemini and Hochberg procedure for multiple testing.

Genes coding cone opsins were excluded because they can be derived from contamination of cones or misalignment of rhodopsin transcripts which are expressed in rods the most abundantly.

Table 2 Significantly enriched pathways of up-regulated genes in the ES1-expressing rods

Pathway	number of genes (O)	expected number of genes (E)	ratio of enrichment (O/E)	P value	Q value
Cytoplasmic ribosomal proteins	8	2.36	3.40	0.0023	0.018
Electron transport chain	7	2.04	3.43	0.0040	0.018
Oxidative phosphorylation	5	1.27	3.95	0.0080	0.024

Adjustment of statistical significance levels for multiple testing was performed by Benjamini and Hochberg procedure, Q<0.05.
Minimum number of genes for a pathway was five.

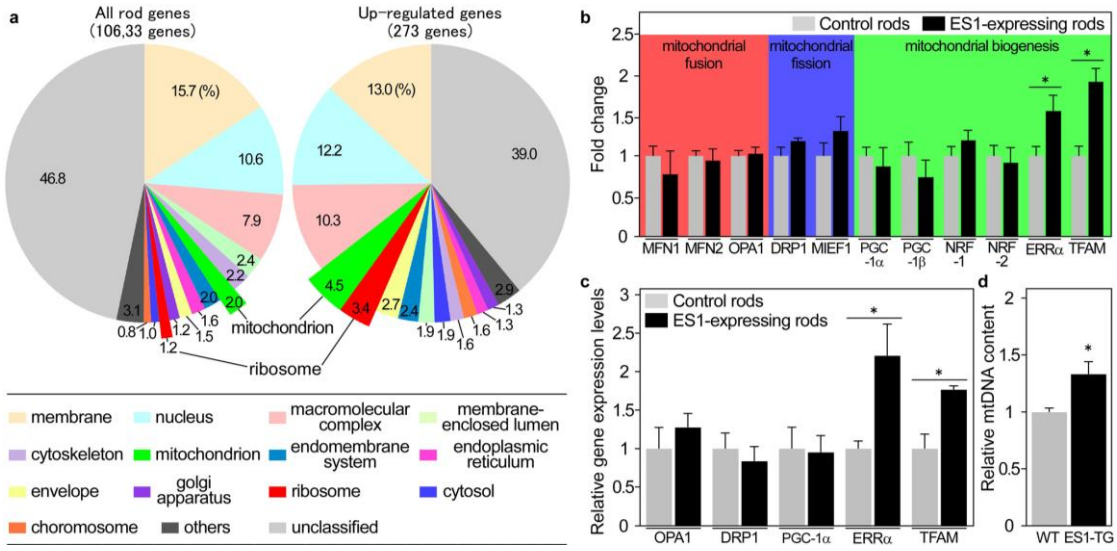

Figure 15 Gene expression changes associated with ectopic expression of ES1 in rods.
(a) Composition of cellular component category based on GO slim classification for all genes detected from the ES1 and/or EGFP-expressing rods (left) and >1.5 fold up-regulated genes in the ES1-expressing rods (right). Proportion of genes classified into ribosome and mitochondrion categories were remarkably increased in the up-regulated genes. (b) Relative gene expression levels of mitochondrial fusion, fission and biogenesis-related genes in the ES1-expressing rods compared with those in the EGFP-expressing rods as a control. Abbreviations: MFN; mitofusin, OPA; optic atrophy, DRP; dynamin-related protein, MIEF; mitochondrial elongation factor, PGC; proliferator activated receptor gamma coactivator, NRF; nuclear respiratory factor, ERR; estrogen-related receptor, TFAM; mitochondrial transcription factor A. Values are means ± S.E. calculated from Cufflinks results for each replicate. *P <0.05 adjusted by Benjamini and Hochberg procedure, n=3 for both control and ES1-expressing rods. (c) Validation of relative expression levels of essential genes for mitochondrial fusion, fission and biogenesis by real-time PCR. Values are means ± S.E., *P <0.05 in Student's t-test, n=3 for both control and ES1-expressing rods. (d) Quantification of mtDNA by real-time PCR in rods purified from ES1-TG or wild-type siblings. Values are means ± S.E., *P =0.04 in Student's t-test, n=3 for both wild-type and ES1-expressing rods.

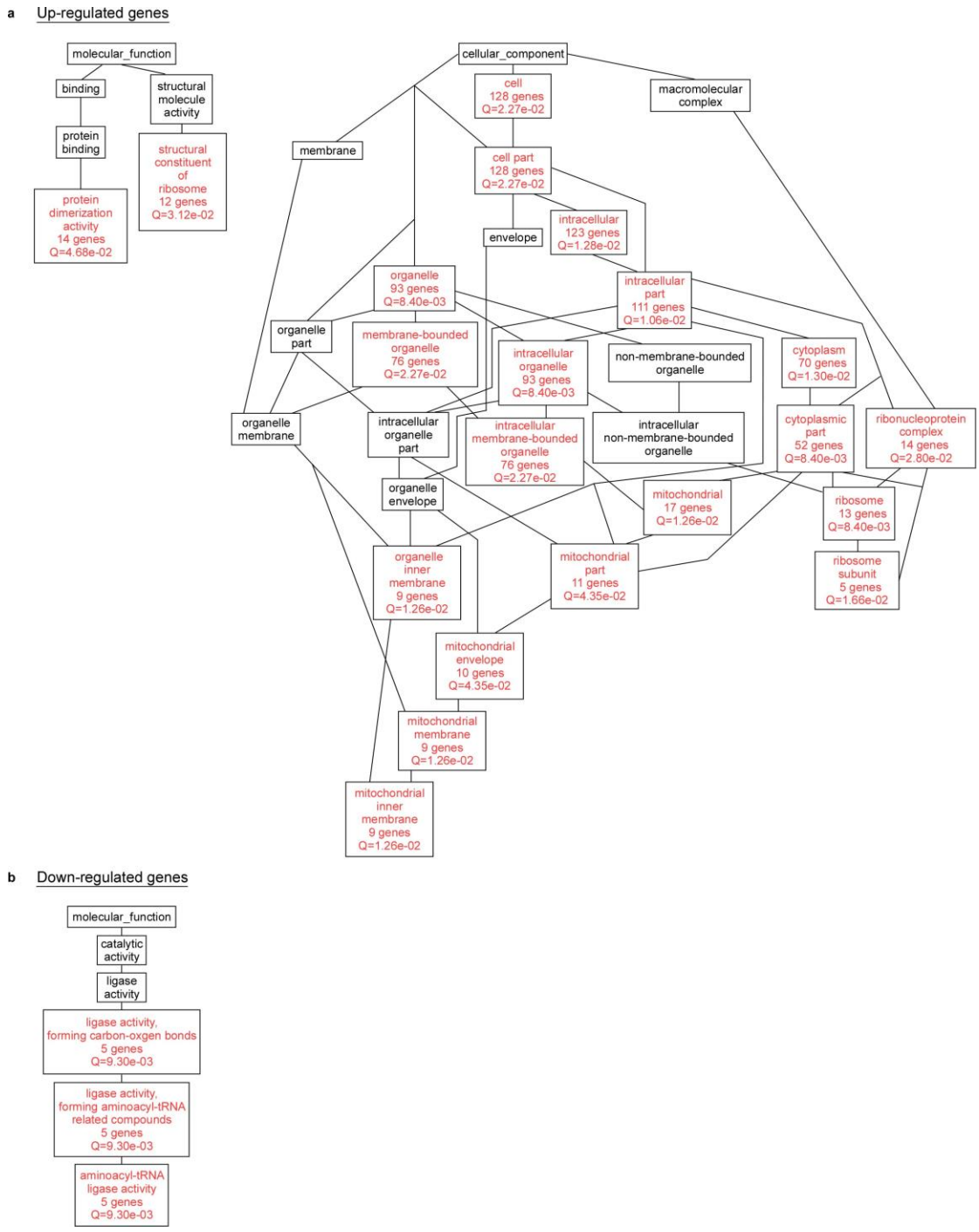

Figure 16 Directed acyclic graph of the enriched GO categories of differentially expressed genes in EGFP-expressing rods.

GO analysis based on the RNA-seq data was performed for >1.5 fold up-regulated genes (a) and > 1.5 fold down-regulated genes (b). Significantly enriched and no-enriched GO categories are coloured red and black, respectively. Multiple test adjustment: Benjamini and Hochberg procedure, Q >0.05, minimum number of genes for a GO category: 5.

Key transcription factors required for mitochondrial biogenesis, such as estrogen-related receptor alpha (ERRα, Villena JA and Kralli A, 2008) and mitochondrial transcription factor (TFAM, Lezza AMS, 2012), were significantly up-regulated (Fig. 15b, c), suggesting that mitochondrial biogenesis was facilitated in the ES1-expressing rods. Consistent with the up-regulation of TFAM, which is also known to play an essential role to regulate mitochondrial DNA (mtDNA) content (Lezza AMS, 2012), the ES1-expressing rods contained significantly higher amount of mtDNA than the wild-type rods (Fig. 15d). Expressions of fusion- and fission-related genes were unchanged in the ES1-expressing rods (Fig. 15b, c), suggesting fusion-independent mitochondrial enlargement.

As to the down-regulated genes, aminoacyl-tRNA ligase was the only significantly overrepresented GO term and no significantly enriched pathway was detected (Fig. 16b).

ES1 expression led to high energy state in rods.

Mitochondrial enlargement is also observed in tissues under pathological conditions such as aged liver, kidney under various clinical states and liver in various experimental conditions (Wakabayashi T, 2002). Hydrazine- or ethanol-treated rat livers contain enlarged mitochondria, and those mitochondria have exhibited low rate of both oxygen consumption and phosphorylating abilities (Wakabayashi T, 2002), indicating low ATP production ability of the mitochondria in such aberrant cells. To investigate whether the mitochondria enlarged by ES1 possess low ATP production ability like the pathologically and pharmacologically enlarged mitochondria or not, I estimated the cellular energy state in ES1 expressing rods. Rods purified with a Percoll density-gradient method either from ES1-TG or wild-type were subjected to assessment of AMPKα phosphorylation level which is an indicator of cellular energy states: in response to an elevated AMP/ATP ratio (low energy state), AMPKα is phosphorylated at Thr172 (in human AMPKα) and activated (Carling D *et al*, 2011). The phosphorylation level of AMPKα in ES1-expressing rods was suppressed by 60% of that in the wild-type rods (Fig. 17a, b), representing a high energy state in the

ES1-expressing rods. Note that no contamination of cones was detected in the purified rod fractions (Fig. 17c). Consistently, measurement utilizing luciferase activity showed that cellular ATP levels in ES1-expressing rods were approximately two-fold higher than that in wild-type rods (Fig. 17d). These results indicate that the mitochondria enlarged by ES1 are capable of high ATP production in rods. Consequently, I propose that ES1 supports mitochondrial energy production in cones via mitochondrial enlargement. I also propose that distinct mechanisms could underlie the mitochondrial enlargement between cones and the aberrant cells.

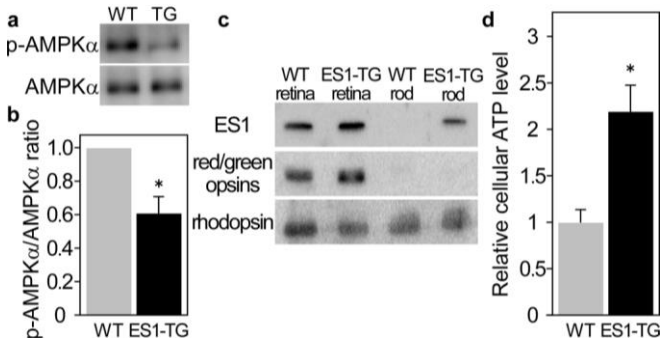

Figure 17 ES1-enhanced mitochondrial energy production in rods.
(a) A representative result of immunoblottings with antibodies against AMPKα and phospho-AMPKα for estimation of phosphorylation levels of AMPKα in rods isolated from ES1-TG or WT siblings. (b) Relative phosphorylation levels of AMPKα in isolated rods assessed by the immunoblottings. Values are means ± S.E., *P=0.008 in Student's t-test, n=7 for both WT and ES1-TG. (c) Immunoblottings of both the retinas and rods isolated from ES1-TG or WT siblings with antibodies against ES1, red/green opsins or rhodopsin. (d) Relative ATP levels in an isolated rod. Values are means ± S.E., *P=0.002 in Student's t-test, n=8 for both ES1-TG and WT.

Discussion

In the present study, I revealed the localization and physiological roles of ES1: ES1 is localized in cone mitochondria and contributes to mitochondrial enlargement. Furthermore, ES1 facilitates mitochondrial biogenesis via up-regulation of mitochondrial proteins expression and contributes to produce high ATP in cones via mitochondrial biogenesis. Although molecular functions of ES1 are still largely unknown, I discuss here how ES1 enlarges mitochondria according to my study and previous studies by others.

The size of individual mitochondria has recently been known to be controlled by the balance between mitochondrial fusion and fission (Cerveny KL *et al.*, 2007; Westermann B, 2012). Overexpression of a mitochondrial fusion protein, MFN1, or knocking-out of a mitochondrial fission protein, DRP1 resulted in mitochondrial enlargement (Park KS *et al*., 2008; Ishihara N *et al.*, 2009). However, in both experiments, total mitochondrial mass or cellular ATP levels were not increased, indicating that total mitochondrial mass is unrelated to the mitochondrial fusion or fission. In contrast, in the present study, ectopic ES1 expression in rods enlarged mitochondria with concomitant increase in the total mitochondrial mass (Fig. 12a, b) and the ATP production (Fig. 17) without affecting the number of mitochondria (Fig. 12e), suggesting strongly that ES1-induced mitochondrial enlargement was achieved in a fusion-independent manner. Consistently, the RNA-seq data and the following validation by real-time PCR suggested that mitochondrial fusion was not increased in the ES1-expressing rods (Fig. 15b, c). This idea is supported by a previous report describing that a single mega-mitochondrion was suggested to be formed by enlargement of a single mitochondrion not by the fusion of smaller mitochondria (Knabe W & Kuhn HJ, 1996).

Such a fusion-independent mitochondrial enlargement is seen in mitochondrial biogenesis, which is an essential process to increase total mitochondrial mass. Mitochondrial biogenesis comprises mitochondrial proliferation and growth, and routinely occurs in dividing cells to restore their mitochondrial mass, or alternatively, occurs in response to energy demand after stimulation such as excise

(Sanger N *et al*., 2000; Irrcher I *et al*., 2003). Mitochondrial biogenesis has been known to be regulated by peroxisome proliferator-activated receptor gamma coactivator 1-alpha (PGC-1α) and its downstream genes (Fernandez-Marcos PJ, Auwerx J, 2011; Scarpulla RC, 2011). ES1-induced mitochondrial enlargement is presumably a part of the mitochondrial biogenesis. This idea is supported by phenotypic similarity of loss-of and gain-of function analyses for ES1 in the present study (Fig. 7, 12 and 17) and PGC-1α: knocking-out of both of PGC-1α and PGC-1β reduced both the size of individual mitochondria and the total mitochondrial mass in mouse cardiac myocytes (Lai L *et al*., 2008), and overexpression of PGC-1α induced mitochondrial enlargement with concomitant increase in the total mitochondrial mass, mtDNA content and ATP production in cultured murine myoblasts (Lehman JJ *et al*., 2000). In the ES1-expressing rods, neither PGC-1α nor PGC-1β were up-regulated (Fig. 15b, c), suggesting the mitochondrial biogenesis induced in the rods was caused by ES1 rather than up-regulation of PGC-1s. Previous studies have shown that ES1 gene expression was down-regulated in brain of PGC-1α knockout mice and in murine muscle where PGC-1α was depleted (Cui L *et al.*, 2006; Sczelecki S *et al.*, 2014). On the other hand, overexpression of PGC-1α has up-regulated ES1 gene expression in cultured murine myoblasts (Calvo S *et al*., 2006). Consequently, these facts suggest that ES1 plays important roles in mitochondrial biogenesis in the downstream of PGC-1α.

In mitochondrial biogenesis, expression of mitochondrial protein is necessary to increase mitochondrial mass and to maintain mitochondrial integrity (Scarpulla RC, 2006). Some transcription factors in downstream of PGC-1α, such as NRF-1, NRF-2, and Errα, are known to regulate nuclear-encoded mitochondria related genes (Hock MB & Kralli A, 2009; Scarpulla RC *et al*., 2012). The ectopic expression of ES1 in rods up-regulated Errα (Fig. 15b, c), which is a well-established transcription factor. Brown adipose tissue (BAT) of Errα null mice showed decreased mitochondrial mass (Villena JA *et al.*, 2007), and overexpression of ERRα increased mitochondrial mass in rat neonatal cordial myocytes and C2C12 myocytes (Huss JM, *et al*., 2004; Murray J & Huss JM, 2011). A number of mitochondria related genes were up-regulated in the

ES1-expressing rods (Fig. 15a, Fig. 16a and Table 2), and the major part of these genes (*ckmt2, coq4, cox6a1, gfm1, gfm2, glrx5, got2a, ndufa6, ndufs1, ndufs3, mrps30,* and *uqcrq*) is predicted as direct transcriptional targets of ERRα (Giguère V, 2008; Deblois G *et al.*, 2009; Charest-Marcotte A *et al.*, 2010; Tremblay AM *et al.*, 2010). In addition, TFAM, which has also been known to be a downstream gene of ERRα (Schreiber SN *et al.*,2004), was up-regulated in the ES1-expressing rods (Fig. 15b, c). Since TFAM is a major transcription factor for mtDNA-encoded genes, expression of the mtDNA-encoded genes would be enhanced in the ES1-expressing rods. Collectively, our data strongly suggest that ES1 enhances expressions of both the nuclear and mtDNA-encoded mitochondrial genes to facilitate mitochondrial enlargement via up-regulation of ERRα.

Although the expression of ES1 is restricted in cones (Fig. 3), ES1 paralogue (NCBI's official symbol is zgc: 112056), which possesses a putative MLS at the N-terminus, is expressed in diverse tissues as described above. Similarly, human and mouse orthologues of ES1 are also expressed in diverse tissues, especially in tissues with high metabolic demands such as heart, kidney and muscle (NCBI, Unigene cluster; Hs.413482, Mm. 268691). These tissues exhibit high expression of PGC-1α, and possess much and large mitochondria. The orthologues are also considered to be localized in mitochondria (Mootha VK *et al.*, 2003). These facts imply that ES1 homologues are also involved in mitochondrial biogenesis in diverse cell types. Their physiological roles remain to be understood.

Although the roles of mega-mitochondria observed in cones have been suggested previously, it remains unclear. Mega-mitochondria in tree shrew cones have been hypothesized to concentrate light onto the outer segments (Knabe *et al.*, 1997), or to improve signal detection (Hárosi FI & Novales FI, 2012). Huge mitochondria, called as ellipsosomes, in cones of atlantic silverside fish and killifish have been suggested to act as a light filter (Novales FI & Hárosi FI, 1999; Novales FI & Hárosi FI, 2000). On the other hand, Tarboush R *et al.* proposed that mega-mitochondria in zebrafish cones may serve to enhance energy production for photoreceptor function and/or exert a protective role by decreasing apoptosis via oxidative stress rather than

light filtering (Tarboush R *et al*., 2014). In the present study, I show that enlarged mitochondria by ES1 were capable of high ATP production in rods, supporting the idea that mega-mitochondria in cones serve to enhance energy production. Sensitivity of oxidative stress or light absorbance of the enlarged mitochondria by ES1 should be investigated.

While MO-mediated ES1 knockdown induced reduction in size of cone mitochondria (Fig. 8), CRISPR/Cas 9 mediated ES1 KO induced apoptotic cell death (Fig. 10f, g). These results suggest that cones possessing small amount of ES1 display reduction of mitochondrial size, and cones completely lacking ES1 undergo apoptosis. Thus, I speculate that ES1 is necessary for nascent cone alive. Experiments using F_1

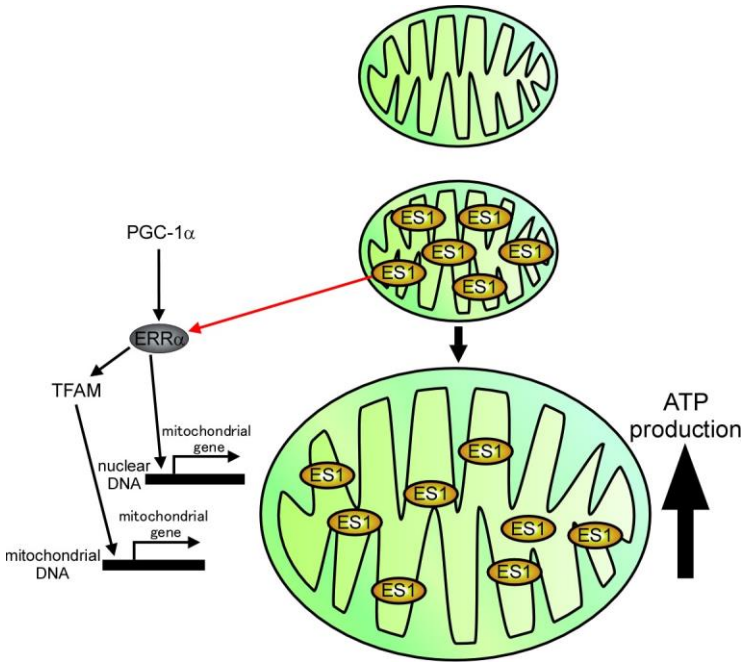

Figure 18 Schematic model of ES1 role and relationship between ES1 and mitochondrial biogenesis-related factors.

ES1 contributes to enlargement of individual mitochondrion (green). ERRα, whose expression is under control of PGC-1α, is up-regulated by ES1 and induces expression of nuclear encoded-mitochondrial genes and mtDNA encoded-mitochondrial genes via TFAM expression. Expressions of these mitochondrial genes would facilitate mitochondrial biogenesis.ES1 facilitates ATP production via mitochondrial biogenesis. Thin allows indicate direct or indirect transcriptional controls. The pathway newly suggested in this study is indicated in red.

ES1 KO are required for further investigation of ES1 roles for mitochondria and apoptosis.

Despite a large number of recent studies on mitochondrial biogenesis, molecular mechanisms underlying enlargement of individual mitochondria during the mitochondrial biogenesis have been largely unknown. To my knowledge, no mitochondrial proteins have been reported to promote the mitochondrial enlargement. The present study led me to conclude that ES1 is the mitochondrial protein that is first found to promote the mitochondrial enlargement during mitochondrial biogenesis in a fusion-independent manner in zebrafish cones.

Materials and Methods

Zebrafish.

Zebrafish of wild type Tübingen long fin (TL) line were subjected to my all experiments. Fish were reared in a continuous flow system (REI-SEA; IWAKI, Tokyo) at 28°C under a 14 h light-10 h dark cycle, and larvae were reared in culture dishes with egg water (0.03% Rei-sea marine salt (IWAKI, Tokyo) and 1 mg/L Methylene Blue (JAPAN PET DESIGN CO., LTD, Tokyo) in distilled water) at 28°C. Adult fish and larvae (5-10dpf) were fed live brine shrimps hatched from brine shrimp eggs (A and A MARINE LCC, Salt lake city, Utha, USA) and powdered fish food (Hikari Crest; Kyorin, Hyogo, Japan), respectively. All experimental protocols were approved by my institute (approval number, FBS 14-006). All experimental procedures involving animals and their care were carried out in accordance with the Osaka University Guidelines for Animal Experimentation and the National Institutes of Health Guide for the Care and Use of Laboratory Animals. In all experiments using TG or MO-injected zebrafish, control fish were treated for the same experimental procedure in parallel at the same time points.

RT-PCR.

Total RNAs were extracted from adult zebrafish tissues, whole embryos and a single eye of embryos with TRI REAGENT (Sigma-Aldrich) according to the manufacture's instruction. Ultra Pure glycogen (Invitrogen) was used as a carrier for isopropanol precipitation. The purified RNAs were reverse transcribed by SuperScript III reverse transcriptase (Invitrogen). Amplification of cDNAs was performed in a thermal cycler (Master cycler gradient, Eppendorf, Germany). In all RT-PCR assays, I performed nested PCR with two primer sets:
5'-GCACGAGGTCACTTTATCTCTC-3' (forward primer) and
5'-AGAGGAGCCATGCTGGACAA-3' (reverse primer) were used for the first round of the amplification, and 5'-AGTAAATCAGTCATGTTGGCATCTC-3' (forward primer) and 5'-TGGAGCAAAGATCTGAAAACGG-3' (reverse primer) were used for the second round.

Antibodies.

Anti-ES1, mAAT, rhodopsin and red/green opsins antibodies were prepared in our laboratory or raised commercially. Antigens used for production of each antibody were purified carp ES1 (AB794660, Komatsu Y, 2006), a peptide fragment of carp mAAT (Ser28-Lys428; AB793727), purified carp rhodopsin, a partial peptide of the sequence conserved in carp red and green opsins (STSKTEVSSVAPA; AB055656.1 and AB110602.2, respectively) and partial peptide of anti-cone-type arrestin-1 and -2 corresponding to amino acid residues 66-102 and 68-110, respectively (Tomizuka *et al*., 2015). The other antibodies used were commercially available; anti-α-tubulin (Sigma-Aldrich), anti-TOM20 (Santa Cruz Biotechnology, inc.), anti-AMPKα (Cell Signaling Technology) and anti-phospho-AMPKα antibodies (Cell Signaling Technology). Each antibody was used at the following dilutions for immunoblotting; anti-ES1 (1:1,000), anti-α-tubulin (1:1,000), anti-mAAT (1:1,000), anti-TOM20 (1:1,000), anti-red/green opsins (1:3,000), anti-rhodopsin (1:3,000), Arrestin-1 and -2 (1:300), anti-AMPKα (1:300) and anti-phospho-AMPKα (1:300), for immunohistochemistry; anti-ES1 (1:500), anti-mAAT (1:300), anti-TOM20 (1:300) and anti-red/green opsins (1:500) and for immunocytochemistry; anti-cone-type arrestin-1 (1:300) and -2 (1:300).

***In situ* hybridization.**

In situ hybridization was performed using 10-μm frozen ocular sections prepared from light-adapted zebrafish as previously described (Wada Y *et al*., 2006). In brief, the frozen sections on the slide were pre-treated in TE (10 mM Tris-HCl, 20 mM EDTA, pH 7.5) with 15 μg/ml proteinase K for 15min at 37°C, and fixed with 4% (w/v) paraformaldehyde in phosphate buffer (PB, 140 mM NaH_2PO_4 and 50 mM Na_2HPO_4, pH 7.4) for 5min on ice. Next, these sections were hybridized with digoxigenin-labeled RNA probes for 16h at 45°C. The hybridized probe was detected with alkaline phosphatase-conjugated anti-digoxigenin antibody (Roche Diagnostics K.K.), and visualized by a colour product from substrates 5-bromo-4-chloro-3-indolyl

phosphate and nitro blue tetrazolium. Complementary RNA probes against ES1 mRNA at 372-755 bases of open reading frame and rhodopsin mRNA at 718-936 bases were synthesized by using DIG RNA Labeling Kit (Roche Diagnostics K.K.). Noncomplementary RNA probes against the same region of these genes were used as negative control (sense prove).

Subcellular fractionation.

Cells dissociated from retinas were suspended in a potassium gluconate buffer (115 mM potassium gluconate, 2.5 mM KCl, 2 mM MgCl2, 10 mM HEPES, 0.2 mM EGTA, 0.1 mM CaCl2, pH 7.5). After freeze-thawed three times, the cells were centrifuged at 100,000 x g for 10 min three times and fractionated into supernatant as a soluble fraction and precipitation as a membrane fraction.

Immunohistochemical studies.

Immunohistochemistry was performed using 10-μm frozen sections as previously described (Wada Y *et al*., 2006). Briefly, frozen sections were incubated with 1% (v/v) normal goat serum (Vector Laboratories, Burlingame, CA, USA) in PBS (20 mM phosphate, 150 mM NaCl, pH 7.4) containing 0.2% (v/v) Triton X-100 for 1 h at room temperature. After washing with PBS, the sections were incubated with first antibodies in PBS containing 0.2% (v/v) Triton X-100 at 4°C overnight. After reaction with second antibodies for 1 h at room temperature, the slides were mounted with Vectashield Mounting Media with DAPI (Vector Laboratories, Inc) to stain nuclei. Fluorescent images were obtained with a BX-51 fluorescence microscope and a FluoView FV1000 confocal laser microscope (Olympus Corp., Tokyo, Japan). Signal intensities in the confocal images were determined by the aid of software imageJ (version 1.45, National Institutes of Health, Bethesda, MD). Secondary antibodies used are anti-mouse IgG and anti-rabbit IgG which are conjugated with either Alexa Fluor 488 (1:300 dilution, Molecular probes), Alexa Fluor 568 (1:300 dilution, Molecular probes) or ATTO 655 (1:200 dilution, Sigma-Aldrich).

Preparation of ultrathin sections.

Light-adapted zebrafish were used for electron microscopic analyses. Whole embryos or eyecups from adult zebrafish were fixed with 1% (w/v) paraformaldehyde and 2.5% (w/v) glutaraldehyde in Ringer's solution (4 mM HEPES, 120 mM NaCl, 2.5 mM KCl, 2.5 mM $CaCl_2$, 2.5 mM $MgCl_2$, 16 mM Glucose, 0.5 mM $MgSO_4$, 1 mM $NaHCO_3$, 0.5 mM NaH_2PO_4) for 2 h at 4°C, followed by treatment with 0.5% osmium tetroxide in Ringer's solution for 30 min at 4°C. After dehydration through a graded ethanol series, the tissue fragments were embedded either in epoxy resin Quetol 812 (Nissin EM) or LR-White (for immunoelectron microscopy, London Resin Company), and were cut into ultrathin sections (80-100 nm) by using an ultramicrotome (EM-Ultracut UCT; Leica, Germany). After immunostaining process described below or without the immunostaining, the sections were post-stained with 4% uranyl acetate solution and lead staining solution (Sigma-Aldrich), and observed by using an electron microscope (JEM-1011; JEOL, Tokyo, Japan).

Immunoelectron microscopy.

Immunostaining of the ultrathin sections were performed as described elsewhere (Yamasita S *et al*., 2009) with minor modifications. Briefly, the sections were incubated in an activating buffer (20 mM Tris-HCl, 0.15 M NaCl, pH 9.0) at 95°C for 1 h followed by incubation in a blocking solution containing 1% (w/v) bovine serum albumin in TBS (20 mM Tris-HCl, 0.15 M NaCl, pH 7.4) for 30 min at room temperature. The sections were then incubated with anti-TOM20 antibody (1:800 dilution) in the blocking solution at 4°C overnight. After washing in the blocking solution, the sections were incubated with anti-mouse IgG-conjugated with colloidal-gold (10 nm diameter, British Biocell International, 1:60 dilution) in the blocking solution for 30 min at room temperature. After washing in TBS, the sections were fixed with 0.1 M PB (pH 7.4) containing 1% (w/v) glutaraldehyde at room temperature for 10 min. Then the sections were washed in PB three times, in distilled water once, and then post-stained as described above.

MO-mediated ES1 knockdown.

Two types of MOs against ES1 transcript were synthesized by Gene Tools LLC (Fig. 6A). The sequence of ES1-MO1 was 5'-CAGAGAAAACCTTCAACAGCGCAGA -3', and ES1-MO2 was 5'-AGAGCCCGTGATGCCAACATGACTG-3'. Standard control MO (Gene Tools LLC) was used as a negative control. Knocked-down zebrafish were obtained by injecting with 4.2ng of these MOs into zebrafish embryos at 1-4 cell-stage. Microinjection was performed with an electric microinjector (Narishige im-30; Narishige, Japan) using glass capillary tubes made by pipette puller (P-97 IVF; Sutter, Novato, CA). The embryos were reared at 28°C and subjected to phenotypic analyses at 4 dpf.

Genaration of sgRNA for CRISPR/Cas9 system.

I designed two type of sgRNAs (sgRNA-ES1-1 and -2) on the first exon of ES1 using CRISPRdirect (Naito Y *et al.*, 2014, http://crispr.dbcls.jp/.), which is software for designing sgRNA with reduced off-target sites. The targeted genomic sequence of sgRNA-ES1-1 was 5'- TGGCTGCGGCCTGCTTGGCGAGG -3', and sgRNA-ES1-2 was 5'-TGCCTGCCTGATGCATCACGGGG-3'. Three bases at 3' of both sgRNA ES1-1 and –2 targeting sequences (AGG and GGG, respectively) are the protospacer adjacent motif (PAM) sequence required for Cas9 of *S. Pyogenes* activity. Generation of theses sgRNAs using T7 MEGAscript kit (Life Technologies) was performed as previously described (Auer TO *et al*., 2014). Synthesized sgRNAs were purified with RNeasy mini kit (QIAGEN) according to the manufacture instruction. Estimation of the sgRNA amount was performed using Agilent 2100 bioanalyzer with RNA Pico Chips (Agilent Technologies).

CRISPR/Cas9-mediated ES1 knockout.

I tried to obtain ES1 KO zebrafish using CRISPR/Cas9 system. I injected 125 ng Cas9 mRNA (TriLink BioTechnologies) and various amounts of sgRNAs with 0.05% phenol red into 1-cell stage zebrafish eggs. Evaluation of mutations induced by

the injection was performed with T7E1 assay as previously described (Auer TO *et al*., 2014). Briefly, to extract genomic DAN, injected embryos at 24 hour past fertilization (hpf) were incubated in Lysis buffer (10 mM Tris, 2mM EDTA, 0.2% Triton X-100, 100 μg/ml protenase K) at 55℃ overnight and subsequently at 95℃ 2 min. Genomic PCR were performed with the following primer set 5'-AGTAAATCAGTCATGTTGGCATCTC-3' (forward primer) and 5'-CCCGACTACATGTAAGTACTGATCTC-3' (reverse primer). The PCR products were re-annealed by sequential incubation at 95℃ 5 min, at 85℃ 20sec and 25℃ 20sec, and incubated with T7 endonuclease I (New England Biolabs, Japan) at 37℃ 2h. The re-annealed PCR products were also subjected to electrophorese with acrylamide gel for HMA (Zhu X *et al*. 2014). Mutation efficiency was assessed by TA cloning-based sequencing analysis.

TUNEL assay.

Apoptotic cells in 3dpf larvae retina were detected by TUNEL assay with In Situ Cell Death Detection kit (Toyo Ink, Tokyo, Japan) using 10-μm frozen sections prepared as described in Immunohistochemical studies in Methods. The sections were fixed in PBS containing 4% (w/v) paraformaldehyde for 1 h at room temperature. After washing with PBS, the sections were incubated with 0.1% (w/v) sodium citrate solution on ice for 2 min and with detection solutions contained in the kit at 37℃ for 1 h.

Generation of transgenic zebrafish.

I used *Tol*2 tranposon system (Kawakami K *et al*., 2004; Urasaki A *et al*., 2006) to generate TG zebrafish. *Tol*2-based expression vectors were constructed as shown in Fig. 8A. Approximately 1 nl of an injection solution (5 mM HEPES, pH 7.6, 150 mM KCl, 0.05% phenol red, 25 ng/μl plasmid DNA of each expression construct and 25 ng/μl *Tol*2 transposase mRNA) was injected into fertilized eggs. The embryos were reared at 28℃ and founder larvae were selected with the aid of fluorescence of EGFP in the eyes.

Isolation of rods by Percoll density-gradient centrifugation.

To assess the cellular energy state in rods, adult zebrafish were dark adapted more than 3 h, and following manipulations were performed under dim red light. Retinas were isolated and gently shaken in Ringer's solution to isolate rods. The rods were then purified by Percoll density-gradient centrifugation (Tachibanaki S *et al*, 2001) at 10,000 x g for 10 min, and collected from a boundary between 45% and 60% (w/v). The collected rods were composed of outer segments and ellipsoids but not cell bodies or synaptic termini. The rods were then precipitated by a serial centrifugations; 600 x g for 12 s followed by 3,000 x g for 4 s. The precipitate was suspended in Ringer's solution and used to estimate both the phospho-AMPKα and the cellular ATP levels.

FACS.

To obtain rod mRNAs, which are mainly distributed in cell bodies containing nuclei, rods with cell bodies were fractionated by FACS. To avoid effects of both circadian rhythm and diet for subsequent RNA-seq, I carried out sampling for all fish after 5h of their lunch. Retinas isolated from 15-18 adult fish of the ES1-TG and EGFP-TG were chopped and incubated at room temperature for 15 min in Ringer's solution with 10 Wünsch Units/ml liberase (Roche) and 20 U/ml hyaluronidase (Sigma-Aldrich) to dissociate into single cells. The cells were precipitated by centrifugation at 500 x g for 2 min and resuspended in Ringer's solution. Rod cell bodies were sorted by EGFP signal intensity and size (forward scatter) using BD FACS Aria III flow cytometry (BD Bioscience). The FACS Aria was adjusted with Accudrop beads (BD Bioscience, USA) for the optimum sorting conditions. To obtain fresh mRNA samples, sorted cells were immediately centrifuged at 2,000 x g for 30 sec to remove supernatant and frozen in liquid nitrogen until subsequent mRNA preparation for RNA-seq and quantitative real-time PCR.

Sequencing library preparation.

Purification of poly(A)-containing mRNA was performed with Dynabeads® mRNA DIRECT™ Micro Purification Kit (Life Technologies) according to the manufacturer's protocol. Quantitative estimation and quality check of the mRNA were performed using Agilent 2100 bioanalyzer with RNA Pico Chips (Agilent Technologies). The purified mRNA samples with RNA integrity number (RIN, Schroeder A *et al.*, 2006) value > 8.0 were subjected to subsequent sequencing analysis.

Sequencing by next generation sequencing (NGS).

Prepared mRNA samples were sequenced by Ion PGM device with Ion total RNA-seq kit v2, Ion PGM Template OT2 kit, and Ion PGM 200 Sequencing kit v2 (Life Technologies) according to the manufacturer's protocol. In brief, the mRNA samples were digested using RNase III into fragment with 100-400 bases. The fragmented mRNAs were purified, and then hybridized and ligated with Ion adaptors. Subsequently, they were reversetranscribed and amplified to double-stranded cDNAs. After purification of the cDNAs using maginetic beads, their concentrations were estimated by Agilent 2100 bioanalyzer with DNA Pico Chips (Agilent Technologies). The cDNA libraries were diluted into optimal concentrations and then subjected to Emulsion PCR. Finally, enriched DNA-positive beads were subjected to high-throughput sequencing with an Ion Torrent PGM sequencer (Life Technologies).

Computational analysis for RNA-seq data.

Using the sequenced reads by NGS, expression level of each gene was estimated with computational tools. Firstly, short reads with less than 40 bases and low-quality reads where at least 30% of bases have a Phred score less than 17 were excluded by FastX-Tool kit (http://hannonlab.cshl.edu/fastx_toolkit/). The rest reads were subsequently mapped to the zebrafish reference genome (Zv9) from Ensembl database (http://www.ensembl.org/Danio_rerio/Info/Index) using TopHat2 software (v2.0.11, Kim D *et al.*, 2013). Gene expression levels were then quantified by Cufflinks software (v2.2.1, Trapnell C *et al.*, 2012) as fragments per kilobase of exon

per million mapped sequence reads (FPKM), and differentially expressed genes between each transgenic line condition were determined by Cuffdiff software (Trapnell C *et al.*, 2012). Three replicates for each condition were subjected to these analyses. According to the Cuffdiff result, the variance among the replicates was estimated using the R package CummeRbund (v2. 8. 2, Goff L *et al.*, 2012). The sequence dataset was submitted to the DDBJ Sequence Read Archive (DRA) under accession number DRA004229 with the following BioProject accession number PRJDB4416 and BioSample accession numbers SAMD00044052-SAMD00044057.

GO and pathway enrichment analyses.

Based on the Cuffdiff result, more than 1.5 fold up- or down-regulated genes were subjected to GO analysis to find out attributes of their products using WEB-based Gene Stet Analysis Toolkit (WebGestalt) database (Wang J *et al.*, 2013; Zhang B *et al*., 2005). Pathway enrichment analysis for these genes was performed by Wikipathways included in WebGestalt. All genes whose expression was detected in rods from ES1-TG and/or rods from EGFP-TG (10,633 genes) were used as reference for these statistical analyses.

Quantitative real-time PCR.

Total RNAs were extracted from the EGFP- and ES1-TG purified rods (see "RNA-seq" in the Materials and Methods) by using TRI REAGENT (Sigma-Aldrich) and treated with RQ1 RNase-Free DNase (Promega). Complementary DNAs synthesized as described above were used for Real-time PCR by Applied Biosystems 7900 HT Fast Real-Time PCR System (Life Technologies) with SYBR Green Realtime PCR Master Mix (TOYOBO) in two technical replicates. Specificities of amplified products in each experiment were validated by melting curve analyses. Expression levels were normalized to that of alpha-tubulin as the internal control. Primer set for ERRα was 5'-AGATGTGGCATCTGGCTACC-3' (forward) and 5'-GCCTACTTTGAGGCACTTGG-3' (reverse), and for the other genes were described previously; alpha-tubulin (McCurley *et al.*, 2008), TFAM (Artuso L *et al.*,

2012), OPA1 (Rahn JJ *et al.*, 2013), DRP1 (Rahn JJ *et al.*, 2013) and PGC-1 (Rahn JJ *et al.*, 2013).

Quantification of mtDNA content.

Purified rods composed of the outer segment and the ellipsoid (see "Estimation of cellular energy states of rods" in the Materials and Methods) were treated with lysis buffer (50 mM Tris–HCl pH 8.5, 1 mM EDTA, 0.5% Tween-20, 200 μg/ml proteinase K) at 55°C for 2 h, and then proteinase K was denatured at 95°C for 10 min. Then DNAs were purified with Fast Gene Gel/PCR Extraction Kit (NIPPON Genetics Co. Ltd., Tokyo, Japan). Mitochondrial DNA contents were quantified by real-time PCR using a primer set for mtDNA encoded NADH dehydrogenase 1 (Artuso L *et al.*, 2012) in two technical replicates. The content of mtDNA was normalized by the number of cells.

Estimation of cellular energy states of rods.

Retinas were isolated from dark-adapted (more than 3 h) adult zebrafish and gently shaken in Ringer's solution to isolate rods under dim red light. The rods were then purified by Percoll density gradient centrifugation (Tachibanaki S *et al*, 2001) at 10,000 x g for 10 min, and collected from a boundary between 45% and 60% (w/v) under dim red light. The collected rods were composed of outer segments and ellipsoids without cell bodies or synaptic termini. The rods were then precipitated by a serial centrifugations; 600 x g for 12 s followed by 3,000 x g for 4 s. The precipitate was suspended in Ringer's solution and used to estimate both the phospho-AMPKα and the cellular ATP levels. ATP levels were measured with a luciferin-luciferase reaction assay method using an ATP assay kit for tissue (Toyo Ink) according to the manufacturer's protocol. Within a 96 well plate (Nunc), signal intensity for luminescence was measured by using LAS2000 imaging system (Fuji Photo Film) with the aid of Image Gauge software (Fuji Photo Film).

References

Alm A (1992) Ocular circulation. In *Adler's Physiology of the Eye*, 9th Edition, eds Hart WM (Mosby, New York), 200–226

Artuso L *et al.* (2012) Mitochondrial DNA metabolism in early development of zebrafish (Danio rerio). *Biochim. Biophys. Acta* 1817: 1002–1011

Asaoka Y, Mano H, Kojima D, Fukada Y (2002) Pineal expression-promoting element (PIPE), a *cis*-acting element, directs pineal-specific gene expression in zebrafish. *Proc Natl Acad Sci USA* 99:15456–15461

Auer TO *et al.* (2014) CRISPR/Cas9-mediated conversion of eGFP- into Gal4-transgenic lines in zebrafish. *Nat Protoc* 9:2823–40.

Calvo S *et al.* (2006) Systematic identification of human mitochondrial disease genes through integrative genomics. *Nature Genet* 38:576–582

Carling D, Mayer FV, Sanders MJ, Gamblin SJ (2011) AMP-activated protein kinase: nature's energy sensor. *Nat Chem Biol* 7:512–518

Cerveny KL *et al.* (2007) Regulation of mitochondrial fusion and division. *Trends Cell Biol* 17:563–569

Chang H, Gilbert W (1997) A novel zebrafish gene expressed specifically in the photoreceptor cells of the retina. *Biochem Biophys Res Commun* 237:84–89

Charest-Marcotte A *et al.* (2010) The homeobox protein Prox1 is a negative modulator of ERRalpha/PGC-1alpha bioenergetic functions. *Genes Dev* 4:537–542

Cui L *et al.* (2006) Transcriptional repression of PGC-1alpha by mutant huntingtin leads to mitochondrial dysfunction and neurodegeneration. *Cell* 127:59-69

Deblois G *et al.* (2009) Genome-wide identification of direct target genes implicates estrogen-related receptor alpha as a determinant of breast cancer heterogeneity. *Cancer Res* 69:6149–6157

Fernandez-Marcos PJ, Auwerx J (2011) Regulation of PGC-1α, a nodal regulator of mitochondrial biogenesis. *Am J Clin Nutr* 93:884S–890S

Giguère V (2008) Transcriptional control of energy homeostasis by the estrogen-related receptors. *Endocr Rev* 29:677–696

Goff L, Trapnell C, Kelley D (2012) CummeRbund: visualization and exploration of Cufflinks high-throughput sequencing data. http://www.bioconductor.org/

Guda C, Fahy E, and Subramaniam S (2004, a) MITOPRED: a genome-scale method for prediction of nucleus-encoded mitochondrial proteins. *Bioinformatics*, 20: 1785–1794

Guda C, Guda P, Fahy E, Subramaniam S (2004, b) MITOPRED: a web server for the prediction of mitochondrial proteins. *Nucleic Acids Res*, 32: W372

Hoang QV, Linsenmeier RA, Chung CK, Curcio CA (2002) Photoreceptor inner segments in monkey and human retina: mitochondrial density, optics, and regional variation. *Vis Neurosci* 19:395–407

Hock MB, Kralli A (2009) Transcriptional control of mitochondrial biogenesis and function. *Annu Rev Physiol* 71:177–203

Huss JM, Torra IP, Staels B, Giguère V, Kelly DP (2004) Estrogen-related receptor α directs peroxisome proliferator-activated receptor α signaling in the transcriptional control of energy metabolism in cardiac and skeletal muscle. *Mol Cell Biol* 24:9079–9091

Hárosi F I, Novales FI (2012) Functional significance of the taper of vertebrate cone photoreceptors. *J Gen Physiol* 139:159–187

Irrcher I *et al*. (2003) Regulation of mitochondrial biogenesis in muscle by endurance exercise. *Sports Med* 33: 783–793

Ishihara N *et al.* (2009) Mitochondrial fission factor Drp1 is essential for embryonic development and synapse formation in mice. *Nature Cell Biol* 11:958–966

Kageyama GH, Wong-Riley M (1984) The histochemical localization of cytochrome oxidase in the retina and lateral geniculate nucleus of the ferret, cat, and monkey, with particular reference to retinal mosaics and on/off-center visual channels. *J Neurosci* 4:2445–2459

Kawakami K *et al*. (2004) A transposon-mediated gene trap approach identifies developmentally regulated genes in zebrafish. *Dev Cell* 7:133–144

Kim D *et al.* (2013) TopHat2: accurate alignment of transcriptomes in the presence of insertions, deletions and gene fusions. *Genome Biol* 14:R36

Kim J *et al*. (2005) The presence of megamitochondria in the ellipsoid of photoreceptor inner segment of the zebrafish retina. *Anat Histol Embryol* 34:339–342

Kim MJ, Kang KH, Kim CH, Choi SY (2008) Real-time imaging of mitochondria in transgenic zebrafish expressing mitochondrially targeted GFP. *Biotechniques* 45:331–334

Knabe W, Kuhn HJ (1996) Morphogenesis of megamitochondria in the retinal cone inner segments of Tupaia belangeri (Scandentia). *Cell Tissue Res* 285:1–9

Knabe W, Skatchkov S, Kuhn HJ (1997) “Lens mitochondria” in the retinal cones of the tree-shrew Tupaia belangeri. *Vision Res* 37: 267–271

Kok FO *et al*. (2014) Reverse genetic screening reveals poor correlation between morpholino-induced and mutant phenotypes in zebrafish. *Dev Cell* 32: 97–108.

Komatsu Y (2006) 錐体特異的蛋白質 ES1 の局在と機能の解析. master thesis.

Lai L *et al*. (2008) Transcriptional coactivators PGC-1α and PGC-lβ control overlapping programs required for perinatal maturation of the heart. *Genes Dev* 22:1948–1961

Lehman JJ *et al*. (2000) Peroxisome proliferator-activated receptor γ coactivator-1 promotes cardiac mitochondrial biogenesis. *J Clin Invest* 106:847–856

Lezza AMS(2012) Mitochondrial transcription factor A (TFAM): one actor for different roles. *Front Biol* 7:30–39

Linton JD *et al*. (2010) Flow of energy in the outer retina in darkness and in light. *Proc Natl Acad Sci USA* 107:8599–8604

Lluch S, Lo´pez-Fuster MJ, Ventura J (2002) Giant mitochondria in the retina cone inner segments of shrews of genus Sorex (Insectivora, Soricidae). *Anat Rec* 272A:484–490

Ma J *et al.* (2001) A visual pigment expressed in both rod and cone photoreceptors. *Neuron* 32:451–461

McCurley AT, Callard GV (2008) Characterization of housekeeping genes in zebrafish: male-female differences and effects of tissue type, developmental stage and chemical treatment. *BMC Mol. Biol.* 9:102.

Mootha VK *et al*. (2003) Integrated analysis of protein composition, tissue diversity, and gene regulation in mouse mitochondria. *Cell* 115:629–640

Murray J, Huss JM (2011) Estrogen-related receptor α regulates skeletal myocyte differentiation via modulation of the ERK MAP kinase pathway. *Am J Physiol Cell Physiol* 301:C630–C645

Naito Y, Hino K, Bono H, Ui-Tei K (2014) CRISPRdirect: software for designing CRISPR/Cas guide RNA with reduced off-target sites. *Bioinformatics* 31:1120-1123.

Nag TC, Bhattacharjee J (1995) Retinal ellipsosomes: Morphology, development, identification, and comparison with oil droplets. *Cell Tissue Res* 279:633–637

Nasevicius A, Stephen CE (2000) Effective targeted gene ‘knockdown’ in zebrafish. *Nat. Genet.* 26: 216–220

National center for biotechnology information (NCBI), Unigene cluster; Hs.413482, Mm. 268691 and Dr. 82544. http://www.ncbi.nlm.nih.gov/unigene

Novales FI, Hárosi FI (1999) Photoreceptor pigments of the blueback herring (Alosa aestevalis, Clupeidae) and the Atlantic silverside (Menidia menidia, Atherinidae). *Biol Bull* 197: 235–236

Novales FI, Hárosi FI (2000) Photoreceptors, visual pigments and ellipsosomes in the killifish, Fundulus heteroclitus: A microspectrophotometric and histological study. *Visual Neurosci* 17:403–420

Okawa H, Sampath AP, Laughlin SB, Fain GL (2008) ATP consumption by mammalian rod photoreceptors in darkness and in light. *Curr Biol* 18:1917–1921

Park KS *et al*. (2008) Selective actions of mitochondrial fission/fusion genes on metabolism-secretion coupling in insulin-releasing cells. *J Biol Chem* 283:33347–33356

Perkins GA, Ellisman MH, Fox DA (2003) Three-dimensional analysis of mouse rod and cone mitochondrial cristae architecture: Bioenergetic and functional implications. *Mol Vision* 9:60–73

Rahn JJ, Stackley KD, Chan SS (2013) Opa1 is required for proper mitochondrial metabolism in early development. *PLoS ONE* 8: e59218

Ramage L *et al*. (1993) Functional cooperation of mitochondrial protein import receptors in yeast. *EMBO J* 12:4115−4123

Sanger N, Strohmeier R, Kaufmann M, Kuhl H (2000) Cell cycle-related expression and ligand binding of peripheral benzodiazepine receptor in human breast cancer cell lines. *Eur J Cancer* 36: 2157–2163

Scarpulla RC (2006) Nuclear control of respiratory gene expression in mammalian cells. *J Cell Biochem* 97: 673–683

Scarpulla RC (2011) Metabolic control of mitochondrial biogenesis through the PGC-1 family regulatory network. *Biochim Biophys Acta* 1813:1269–1278

Scarpulla RC, Vega RB, Kelly DP (2012) Transcriptional integration of mitochondrial biogenesis. *Trends endocrinol metab* 23:459–466

Schmidt M *et al.* (2003) How does the eye breathe? Evidence for neuroglobin-mediated oxygen supply in the mammalian retina. *J Biol Chem* 278:1932–1935

Schreiber SN *et al.* (2004) The estrogen-related receptor α (ERRα) functions in PPARgamma coactivator 1α (PGC-1α)-induced mitochondrial biogenesis. *Proc. Natl. Acad. Sci. USA* 101: 6472-6477.

Schroeder A, *et al.* (2006) The RIN: An RNA integrity number for assigning integrity values to RNA measurements. *BMC Mol Biol* 7:3

Scott HS *et al*. (1997) Isolation of a human gene (HES1) with homology to an Escherichia coli and a zebrafish protein that maps to chromosome 21q22.3. *Hum Genet* 99:616–623

Sczelecki S *et al.* (2014) Loss of Pgc-1α expression in aging mouse muscle potentiates glucose intolerance and systemic inflammation. *Am J Physiol Endocrinol Metab* 15:E157-67

Shin JH, Weitzdoerfer R, Fountoulakis M, Lubec G (2004) Expression of cystathionine β-synthase, pyridoxal kinase, and ES1 protein homolog (mitochondrial precursor) in fetal Down syndrome brain. *Neurochem Int* 45:73–79

Tachibanaki S, Tsushima S, Kawamura S (2001) Low amplification and fast visual pigment phosphorylation as mechanisms characterizing cone photoresponses. *Proc Natl Acad Sci USA* 24:14044–14049

Tarboush R *et al*. (2014) Variability in mitochondria of zebrafi sh photoreceptor ellipsoids. *Visual Neurosci* 31:11–23

Tomizuka J, Tachibanaki S, Kawamura S (2015) Direct suppression of light-activated visual pigment by arrestin in carp rods and cones. *J. Biol. Chem.* 290: 9399-9411

Trapnell C *et al.* (2012) Differential gene and transcript expression analysis of RNA-seq experiments with TopHat and Cufflinks. *Nat Protoc* 7:562–578

Tremblay AM *et al.* (2010) Physiological genomics identifies estrogen-related receptor alpha as a regulator of renal sodium and potassium homeostasis and the renin-angiotensin pathway. *Mol Endocrinol* 24:22–32

Urasaki A, Morvan G, Kawakami K (2006) Functional dissection of the *Tol*2 transposable element identified the minimal *cis*-sequence and a highly repetitive sequence in the subterminal region essential for transposition. *Genetics* 174:639–649

Varshney GK, *et al.* (2015) High-throughput gene targeting and phenotyping in zebrafish using CRISPR/Cas9. *Genome Res.* 25, 1030–1042.

Villena JA *et al.* (2007) Orphan nuclear receptor estrogen-related receptor alpha is essential for adaptive thermogenesis. *Proc Natl Acad Sci USA* 104:1418–1423

Villena JA, Kralli A (2008) ERRα: a metabolic function for the oldest orphan. *Trends Endocrinol Metab* 19:269–276

Wada Y, Sugiyama J, Okano T, Fukada, Y (2006) GRK1 and GRK7: Unique cellular distribution and widely different activities of opsin phosphorylation in the zebrafish rods and cones. *J Neurochem* 98:824–837

Wakabayashi T (2002) Megamitochondria formation - physiology and pathology. *J Cell Mol Med* 6:497–538

Wang J *et al.* (2013) WEB-based GEne SeT AnaLysis Toolkit (WebGestalt): update 2013. *Nucleic Acids Res* 41:W77–W83

Westermann B (2012) Bioenergetic role of mitochondrial fusion and fission. *Biochim Biophys Acta* 1817(10):1833–1838

Yamasita S, Katsumata O, Okada Y (2009) Establishment of a standardized post-embedding method for immunoelectron microscopy by applying heat-induced antigen retrieval. *J Electron Microsc (Tokyo)* 58:267–279

Zhang B, Kirov S, Snoddy J (2005) WebGestalt: an integrated system for exploring gene sets in various biological contexts. *Nucleic Acids Res* 33:W741–W748

Zhu X *et al*. (2014) An efficient genotyping method for genome-modified animals and human cells generated with CRISPR/Cas9 system. *Sci. Rep.* 4, 6420.

A list of achievements

<投稿論文>

“ES1 is a mitochondrial enlarging factor contributing to form mega-mitochondria in zebrafish cones”

Takamasa Masuda, Yasutaka Wada and Satoru Kawamura

Scientific Reports 6, Article number: 22360 (2016)

doi:10.1038/srep22360

＜学会発表＞

口頭発表

○増田隆昌、 小松裕規、 橘木修志、 和田恭高、 河村 悟

題目 ： 錐体に豊富に発現しているタンパク質 ES1 の機能解析

2009 年度日本動物学会 近畿支部

神戸大学 六甲台キャンパス 2009 年 5 月 30 日

口頭発表

○増田隆昌、 和田恭高、 河村 悟

題目 ：ゼブラフィッシュ錐体の主要なタンパク質 ES1 のノックダウン解析

Knockdown analyses of ES1 ; a major protein in zebrafish cone.

第 80 回大会日本動物学会 静岡大会

静岡県コンベンションアーツセンター「グランシップ」 2009 年 9 月 17 日～2009 年 9 月 19 日

ポスター発表

○増田隆昌、 和田恭高、 河村 悟

題目 ：ES1 はゼブラフィッシュの錐体視細胞においてミトコンドリアのサイズ調節に寄与する

ES1 contributes regulation of mitochondrial size in zebrafish cones.

第 81 回大会日本動物学会 旭川大会

旭川市大雪クリスタルホール 2011 年 9 月 21 日～2011 年 9 月 23 日

口頭発表

○増田隆昌、 和田恭高、 河村 悟

題目 ：ゼブラフィッシュ錐体ミトコンドリアの巨大化に対する ES1 の寄与

視覚科学フォーラム第 16 回研究会
埼玉医科大学 毛呂山キャンパス　2012 年 8 月 24 日～2012 年 8 月 25 日

口頭発表
○増田 隆昌、 和田 恭高、 河村 悟
題目 : ES1 によるゼブラフィッシュ錐体視細胞のエネルギー産生への寄与
Contribution of ES1 to energy production in zebrafish cones.
第 84 回大会日本動物学会 岡山大会
岡山大学 津島キャンパス　2013 年 9 月 26 日～2013 年 9 月 28 日

Acknowledgments

I thank Prof. Koichi Kawakami (National Institute of Genetics, Japan) for a kind gift of plasmid vectors for *Tol*2 transposon system. I also thank members in our laboratory; Assistant Professor Yasutaka Wada for production of DNA construct for ES1-TG. Mr. Yuki Komatsu for the earlier study on carp ES1 including production of anti-ES1 and mAAT antibodies, Dr. Daisuke Arinobu for production of anti-carp rhodopsin antibody, and Ms. JunkoTomiduka for production of anti-cone-type-arrestin-1 and -2.

I extend gratitude to Professor Satoru Kawamura and Assistant Professor Yasutaka Wada for invaluable discussion and suggestion through this study. I thank Mr. Toshihiro Aramaki for instruction on zebrafish genome editing techniques using CRISPR / Cas9 system. I thank Professor Furukawa, Professor Kondo and Research Associate Professor Okamoto for helpful discussion and critical reading of this thesis. And, I thank all members of Kawamura laboratory for various fruitful discussions and supports.